2012-03

# Adaptive Speed Controller for the SeaFox Autonomous Surface Vessel

Hurban, Michael A.

Monterey, California. Naval Postgraduate School


# NAVAL POSTGRADUATE SCHOOL

**MONTEREY, CALIFORNIA**

# THESIS

**ADAPTIVE SPEED CONTROLLER FOR THE SEAFOX AUTONOMOUS SURFACE VESSEL**

by

Michael A. Hurban

March 2012

| | |
|---|---|
| Thesis Advisor: | Vladimir Dobrokhodov |
| Co-Advisors: | Douglas Horner |
| | Sean Kragelund |

**Approved for public release; distribution is unlimited**

THIS PAGE INTENTIONALLY LEFT BLANK

| REPORT DOCUMENTATION PAGE | | | Form Approved OMB No. 0704-0188 |
|---|---|---|---|
| Public reporting burden for this collection of information is estimated to average 1 hour per response, including the time for reviewing instruction, searching existing data sources, gathering and maintaining the data needed, and completing and reviewing the collection of information. Send comments regarding this burden estimate or any other aspect of this collection of information, including suggestions for reducing this burden, to Washington headquarters Services, Directorate for Information Operations and Reports, 1215 Jefferson Davis Highway, Suite 1204, Arlington, VA 22202-4302, and to the Office of Management and Budget, Paperwork Reduction Project (0704-0188) Washington DC 20503. | | | |
| **1. AGENCY USE ONLY** ***(Leave blank)*** | **2. REPORT DATE** March 2012 | **3. REPORT TYPE AND DATES COVERED** Master's Thesis | |
| **4. TITLE AND SUBTITLE** Adaptive Speed Controller for the SeaFox Autonomous Surface Vessel | | **5. FUNDING NUMBERS** | |
| **6. AUTHOR(S)** Michael A. Hurban | | | |
| **7. PERFORMING ORGANIZATION NAME(S) AND ADDRESS(ES)** Naval Postgraduate School Monterey, CA 93943-5000 | | **8. PERFORMING ORGANIZATION REPORT NUMBER** | |
| **9. SPONSORING /MONITORING AGENCY NAME(S) AND ADDRESS(ES)** N/A | | **10. SPONSORING/MONITORING AGENCY REPORT NUMBER** | |
| **11. SUPPLEMENTARY NOTES** The views expressed in this thesis are those of the author and do not reflect the official policy or position of the Department of Defense or the U.S. Government. IRB Protocol number _____N/A_____. | | | |
| **12a. DISTRIBUTION / AVAILABILITY STATEMENT** Approved for public release; distribution is unlimited | | **12b. DISTRIBUTION CODE** A | |

**13. ABSTRACT (maximum 200 words)**

The thesis addressed the control system development for a high-speed surface vessel. In particular, the work utilized modern adaptive control techniques to design a speed following controller for the SeaFox ASV; the vehicle features three distinct speed, regimes including the displacement, rapid transition and planing regimes. The study started with the collection of experimental data required to characterize the operating modes and the inherent nonlinear phenomena of the high-speed ASV. Then, it proceeded to system identification study with an objective to develop a mathematical model of the vehicle thus aiming to represent the ASV's speed dynamics at various regimes and to facilitate control system development. After completing the model development, three speed following controllers were designed: A classical Proportional-Integral-Derivative (PID), a nonlinear Model Reference Adaptive (MRAC) and a $L_1$ Adaptive Controller. The motivation behind the choice of three different controllers is two-fold. First, comparison of the linear and nonlinear control approaches is desired to better illustrate the achievable control architecture limitations. Second, comparing two types of nonlinear adaptive control architectures allowed the selection of the best control algorithm for operating the ASV speed in the presence of highly non-linear dynamics and significant disturbances acting on it. Furthermore, each controller is integrated with the SeaFox mathematical model and implemented with and without realistic operational disturbances. This provided a basis for objective comparison among the controllers and gave a means to demonstrate their relative robustness and performance characteristics. Finally, the MRAC and the PID controller were implemented onboard the actual SeaFox ASV and tested in numerous sea-trials under natural conditions to once again demonstrate the advantages and limitations of the chosen control architectures.

| **14. SUBJECT TERMS** Autonomous, Unmanned, Surface, Vehicle, USV, Control, Throttle, SeaFox, Modeling, Controller, PID, MRAC, L1, ASV, adaptive | | | **15. NUMBER OF PAGES** 87 |
|---|---|---|---|
| | | | **16. PRICE CODE** |
| **17. SECURITY CLASSIFICATION OF REPORT** Unclassified | **18. SECURITY CLASSIFICATION OF THIS PAGE** Unclassified | **19. SECURITY CLASSIFICATION OF ABSTRACT** Unclassified | **20. LIMITATION OF ABSTRACT** UU |

NSN 7540-01-280-5500 Standard Form 298 (Rev. 2-89)
Prescribed by ANSI Std. 239-18

THIS PAGE INTENTIONALLY LEFT BLANK

**Approved for public release; distribution is unlimited**

# ADAPTIVE SPEED CONTROLLER FOR THE SEAFOX AUTONOMOUS SURFACE VESSEL

Michael A. Hurban
Lieutenant, United States Navy
B.S., Thomas Edison State College, 2003

Submitted in partial fulfillment of the
requirements for the degree of

**MASTER OF SCIENCE IN MECHANICAL ENGINEERING**

from the

**NAVAL POSTGRADUATE SCHOOL**
**March 2012**

Author: Michael A. Hurban

Approved by: Vladimir Dobrokhodov
Thesis Advisor

Douglas Horner
Thesis Co-Advisor

Sean Kragelund
Thesis Co-Advisor

Knox T. Millsaps
Chair, Department of Mechanical and Aerospace Engineering

THIS PAGE INTENTIONALLY LEFT BLANK

# ABSTRACT

The thesis addressed the control system development for a high-speed surface vessel. In particular, the work utilized modern adaptive control techniques to design a speed following controller for the SeaFox ASV; the vehicle features three distinct speed, regimes including the displacement, rapid transition and planing regimes. The study started with the collection of experimental data required to characterize the operating modes and the inherent nonlinear phenomena of the high-speed ASV. Then, it proceeded to system identification study with an objective to develop a mathematical model of the vehicle thus aiming to represent the ASV's speed dynamics at various regimes and to facilitate control system development. After completing the model development, three speed following controllers were designed: A classical Proportional-Integral-Derivative (PID), a nonlinear Model Reference Adaptive (MRAC) and a $L_1$ Adaptive Controller. The motivation behind the choice of three different controllers is two-fold. First, comparison of the linear and nonlinear control approaches is desired to better illustrate the achievable control architecture limitations. Second, comparing two types of nonlinear adaptive control architectures allowed the selection of the best control algorithm for operating the ASV speed in the presence of highly non-linear dynamics and significant disturbances acting on it. Furthermore, each controller is integrated with the SeaFox mathematical model and implemented with and without realistic operational disturbances. This provided a basis for objective comparison among the controllers and gave a means to demonstrate their relative robustness and performance characteristics. Finally, the MRAC and the PID controller were implemented onboard the actual SeaFox ASV and tested in numerous sea-trials under natural conditions to once again demonstrate the advantages and limitations of the chosen control architectures.

THIS PAGE INTENTIONALLY LEFT BLANK

# TABLE OF CONTENTS


I. INTRODUCTION....1
A. SEAFOX....1
B. DESIGN REQUIREMENTS....1
C. PROBLEM STATEMENT....2
D. THESIS OBJECTIVES....4

II. DATA GATHERING AND MODELING....5
A. CHAPTER OVERVIEW....5
B. MODELING APPROACH....5
C. DATA GATHERING....6
D. MOTIVATION FOR MODEL STRUCTURE....8
E. SYSTEM IDENTIFICATION....9

III. CONTROLLER DESIGN....17
A. CHAPTER OVERVIEW....17
B. PID CONTROLLER WITH GAIN SCHEDULING....17
C. COMPOSITE MRAC WITH INPUT CONSTRAINTS AND GAIN SCHEDULING....21
D. $L_1$ CONTROLLER....28

IV. SIMULATION AND SEA TRIAL RESULTS....33
A. CHAPTER OVERVIEW....33
B. SIMULATION RESULTS....33
1. Displacement Regime Results....33
2. Planing Regime Results....39
3. Transition Regime Results....44
C. SEA TRIAL RESULTS....48
1. PID Results....48
2. MRAC Results....50

V. CONCLUSIONS....53
A. CHAPTER OVERVIEW....53
B. ANALYSIS....53
1. System Identification and Modeling....53
2. Simulation Results....53
3. Sea Trial Results....54
C. CONCLUSION....54
D. FUTURE WORK....55

APPENDIX A....57
A. SYSTEM IDENTIFICATION TOOLBOX RESULTS....57
B. *FMINSEARCH* PARAMETER RESULTS....58

APPENDIX B....61

APPENDIX C....63

**A. EMBEDDED MATLAB FUNCTION: MAIN.M ..... 63**
**B. EMBEDDED MATLAB FUNCTION: SIMULATION.M ..... 63**

**APPENDIX D. ..... 65**
**A. PID CONTROLLER PARAMETERS ..... 65**
**B. COMPOSITE MRAC CONTROLLER PARAMETERS ..... 65**
**C. $L_1$ CONTROLLER PARAMETERS ..... 65**

**LIST OF REFERENCES ..... 67**

**INITIAL DISTRIBUTION LIST ..... 69**

# LIST OF FIGURES


Figure 1. SeaFox Operating in the Displacement Regime ..... 3
Figure 2. SeaFox Operating in the Planing Regime ..... 3
Figure 3. SeaFox Speed Regimes ..... 4
Figure 4. Speed and Throttle Command Data from Field Experimentation ..... 7
Figure 5. Throttle vs. Speed from Experimental Data Showing Hysteresis ..... 9
Figure 6. Process Models GUI ..... 11
Figure 7. *fminsearch* Parameter Estimation Model ..... 12
Figure 8. Model Comparison with Actual Data for a 0% to 99% Throttle Change ..... 13
Figure 9. Model Comparison with Actual Data for a 85% to 0% Throttle Change ..... 14
Figure 10. SeaFox Throttle Dynamics Model ..... 15
Figure 11. Basic PID Controller Block Diagram (From Åström and Hägglund, 1995) ..... 18
Figure 12. PID Controller with Anti-Windup and Derivative Filtering ..... 19
Figure 13. System Diagram with PID Controller combined with Gain Scheduling and Low-Pass Filter ..... 20
Figure 14. Block Diagram of a Model Reference Adaptive Control (From Ioannou and Fidan, 2006) ..... 22
Figure 15. Composite MRAC ..... 25
Figure 16. Composite MRAC Reference Model ..... 25
Figure 17. Composite MRAC State Predictor ..... 26
Figure 18. Composite MRAC Adaptive Law and Controller ..... 27
Figure 19. $L_1$ Adaptive Controller Block Diagram (From Hovakimyan and Cao, 2010a) ..... 29
Figure 20. $L_1$ Adaptive Controller ..... 31
Figure 21. $L_1$ Control Law ..... 31
Figure 22. $L_1$ Adaptive Law ..... 32
Figure 23. System Response: 3 m/s Reference Command, No Disturbance ..... 34
Figure 24. Controller Response: 3 m/s Reference Command, No Disturbance ..... 35
Figure 25. System Response: 3 m/s Reference Command, Constant Disturbance ..... 36
Figure 26. Controller Response: 3 m/s Reference Command, Constant Disturbance ..... 37
Figure 27. System Response: 3 m/s Reference Command, Oscillatory Disturbance ..... 38
Figure 28. Controller Response: 3 m/s Reference Command, Oscillatory Disturbance ..... 39
Figure 29. System Response: 12 m/s Reference Command, No Disturbance ..... 40
Figure 30. Controller Response: 12 m/s Reference Command, No Disturbance ..... 41
Figure 31. System Response: 12 m/s Reference Command, Constant Disturbance ..... 41
Figure 32. Controller Response: 12 m/s Reference Command, Constant Disturbance ..... 42
Figure 33. System Response: 12 m/s Reference Command, Oscillatory Disturbance ..... 43
Figure 34. Controller Response: 12 m/s Reference Command, Oscillatory Disturbance ..... 43
Figure 35. System Response: 6 m/s Reference Command, No Disturbance ..... 44
Figure 36. Controller Response: 6 m/s Reference Command, No Disturbance ..... 45
Figure 37. System Response: 6 m/s Reference Command, Constant Disturbance ..... 45
Figure 38. Controller Response: 6 m/s Reference Command, Constant Disturbance ..... 46

Figure 39. System Response: 6 m/s Reference Command, Oscillatory Disturbance.....46
Figure 40. Controller Response: 6 m/s Reference Command, Constant Disturbance .....47
Figure 41. System Response: PID Controller Sea Trials .....49
Figure 42. Controller Command: PID Controller Sea Trials .....50
Figure 43. System Response: MRAC Sea Trials .....51
Figure 44. Controller Command: MRAC Sea Trials .....51
Figure 45. Model Comparison with Actual Data for a 0% to 50% Throttle Change.....61
Figure 46. Model Comparison with Actual Data for a 75% to 99% Throttle Change.....61
Figure 47. Model Comparison with Actual Data for a 30% to 0% Throttle Change.....62
Figure 48. Model Comparison with Actual Data for a 99% to 75% Throttle Change.....62

# LIST OF TABLES


Table 1. Results of the System Identification for Acceleration in the Displacement Regime ..... 57
Table 2. Results of the System Identification for Acceleration in the Planing Regime ..... 57
Table 3. Results of the System Identification for Deceleration in the Displacement Regime ..... 58
Table 4. Results of the System Identification for Deceleration in the Planing Regime ..... 58
Table 5. *fminsearch* Parameter Results for Acceleration in the Displacement Regime ..... 58
Table 6. *fminsearch* Parameter Results for Acceleration in the Planing Regime ..... 59
Table 7. *fminsearch* Parameter Results for Deceleration in the Displacement Regime ..... 59
Table 8. *fminsearch* Parameter Results for Deceleration in the Planing Regime ..... 59
Table 9. Parameters of the PID Controller ..... 65
Table 10. Parameters of the Composite MRAC Controller ..... 65
Table 11. Parameters of the $L_1$ Controller ..... 65

THIS PAGE INTENTIONALLY LEFT BLANK

# LIST OF ACRONYMS AND ABBREVIATIONS

| | |
|---|---|
| ASV | Autonomous Surface Vessel |
| CAVR | Center for Autonomous Vehicle Research |
| GPS | Global Positioning System |
| GUI | Graphical User Interface |
| ISR | Intelligence, Surveillance, and Reconnaissance |
| MIO | Maritime Interdiction Operations |
| MRAC | Model Reference Adaptive Controller |
| NPS | Naval Postgraduate School |
| PID | Proportional-Integral-Derivative |
| RHIB | Rigid Hull Inflatable Boat |
| USV | Unmanned Surface Vehicle |

THIS PAGE INTENTIONALLY LEFT BLANK

# ACKNOWLEDGMENTS

Foremost, this work would not have been possible without the advice, guidance and assistance from my thesis advisors, Professor Vladimir Dobrokhodov, Professor Doug Horner and Sean Kragelund. I cannot thank you enough for the patience you have shown during this process.

I would also like to thank Professor Isaac Kaminer for going out of his way to help build the foundation of this thesis. Without your help, I could never have accomplished this.

To Aurelio Monarrez, I owe a debt of gratitude for helping out every time we took SeaFox out. I truly appreciate you taking time out of your personal life to sit with us in the rain.

Finally, to my wife. Thank you for always being there to support me and my career.

THIS PAGE INTENTIONALLY LEFT BLANK

# I. INTRODUCTION

## A. SEAFOX

The SeaFox is a 15′5″ rigid hull inflatable boat (RHIB) originally designed by Northwind Marine. It has a JP-5 fueled water jet propulsion system and is capable of reaching speeds over 30 knots. The SeaFox has the option to be controlled manually, remotely using a handheld controller, or automatically using a GPS-based waypoint guidance system. For this thesis, we consider employment of the RHIB as an Autonomous Surface Vehicle (ASV). Employment possibilities of the RHIB include naval applications such as Riverine Operations, Maritime Interdiction Operations (MIO), Port Security, and Intelligence, Surveillance, and Reconnaissance (ISR) missions according to [1], [2]. Focusing on the Riverine community, the Center for Autonomous Vehicle Research (CAVR) at the Naval Postgraduate School (NPS), in a combined effort with Virginia Tech, are developing capabilities for autonomous reconnaissance in unknown environments. The SeaFox ASV must possess the ability to autonomously navigate in restricted waterway while avoiding obstacles above and below the waterline. This capability would also allow troop or supply movement without the need of a boat crew, thus minimizing the possibility of attack on military personnel. During MIO, a network of autonomous vessels could be used to cooperatively localize and approach suspicious surface vessels without putting service members in harm's way. An overall goal of CAVR is to make the SeaFox ASV a completely autonomous vehicle capable of operating within a network of autonomous vehicles under variable environmental conditions and mission load outs without the need of re-tuning the onboard control system prior to every mission.

## B. DESIGN REQUIREMENTS

To be able to accomplish these missions, the SeaFox ASV must have greater levels of onboard autonomy. This must include the ability to:

1. Build and update an internal representation of the environment through its sensors.

2. Localize its own position with respect to the local operational environment.

3. Determine the optimal path to reach the desired destination.

4. Automatically navigate the recommended course in coordination with other autonomous vehicles.

These basic requirements for a vehicle to be autonomous enable behaviors such as obstacle and vessel tracking and avoidance.

ASV position localization is performed by an onboard Global Positioning System (GPS) and Inertial Measurement Unit (IMU). The other three requirements are being addressed by a joint project for ASV Riverine Autonomy between the Naval Postgraduate School and Virginia Tech. This is being achieved in part using forward looking sonar and a surface scanning laser [3].

An important enabling component of this research is the ability to vary throttle speeds and actuate to the desired speeds with minimal errors. In riverine operations, with potentially significant river currents, a robust throttle controller is a critical component of greater ASV autonomy.

## C. PROBLEM STATEMENT

For most powerboats there are three different operating regimes: displacement, transition, and planing. Marshall [4] states that in the displacement mode, the hull is supported by buoyancy. In the transition region, the hull is still supported predominantly through buoyancy but the hull shape begins to produce hydrodynamic lift as well. In the planing mode almost all of the boat's weight is supported by hydrodynamic lift (Figures 1 and 2).

Figure 1. SeaFox Operating in the Displacement Regime

Figure 2. SeaFox Operating in the Planing Regime

Figure 3 shows a typical speed plot as SeaFox accelerates from 0% to 75% throttle command. It can be seen that there are three distinct regions in which the speed profile can be divided; the displacement and planing regimes with a rapid transition between the two. Even though the SeaFox ASV exhibits the three regime behavior, it only has the ability to operate in the displacement and planing regimes when given a constant throttle command. Past efforts at speed control have been unsuccessful because each regime has very distinct hydrodynamic characteristics which contribute to the nonlinearities in the overall velocity model, thus making conventional control architectures inadequate.

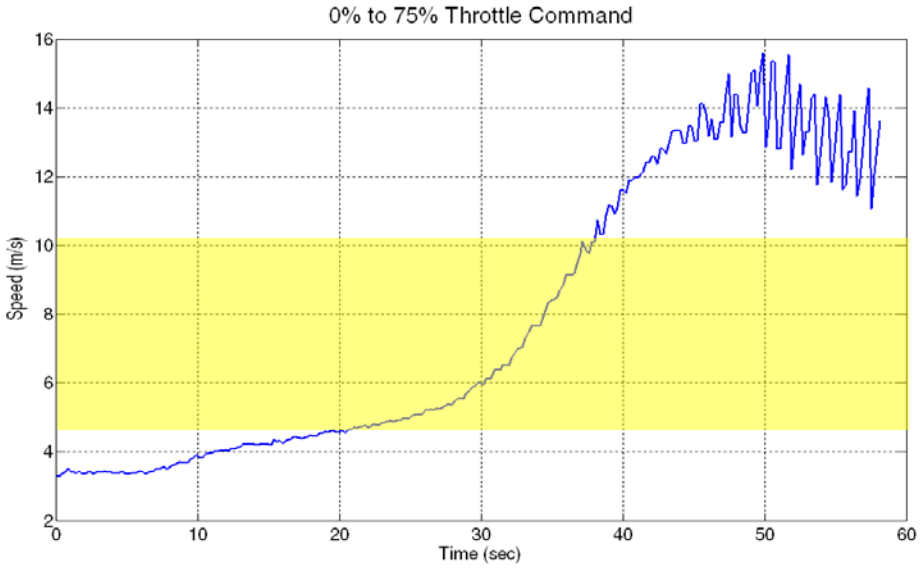


Figure 3. SeaFox Speed Regimes

## D. THESIS OBJECTIVES

The objective of this thesis is to develop and test a single speed controller that will adapt to the hydrodynamics of different operating regimes. To accomplish this, a mathematical model representing SeaFox's throttle versus speed dynamics is developed. The model represents the distinct characteristics of each speed regime. Next, three controllers are developed, namely, a Proportional-Integral-Derivative (PID), a Model Reference Adaptive Controller (MRAC), and a $L_1$ controller. The intent of developing three controllers is to facilitate a comparative study between standard linear control theory (PID) and relatively new adaptive control theory (MRAC and $L_1$). Next simulated trials are presented with the three controllers. Finally, the PID and MRAC controllers are implemented within the control structure of SeaFox and results are presented. The thesis concludes with final remarks and recommendations for future work.

# II. DATA GATHERING AND MODELING

## A. CHAPTER OVERVIEW

This chapter presents an analysis of experimental data collected at Lake San Antonio near Paso Robles, CA. The data is used to implement a mathematical model of SeaFox in a Matlab Simulink environment. The intent is to develop a model which is accurate enough to develop speed controllers capable of accommodating the unique characteristics of the SeaFox ASV.

## B. MODELING APPROACH

Many different approaches have been taken to model surface vessels dynamics. One common approach is to model the vessel dynamics based on equations of motion. Triantafyllou and Hover [5] and Fossen [6] have taken this approach to develop extensive methods for modeling surface vessels using a standard six degree-of-freedom (6DOF) model of the vehicle's dynamics. These models tend to work well when all of the control forces are known and the vessel remains in the displacement regime but as the vessel transitions through regimes, the dynamics change, thereby invalidate the model.

Savitsky [7] has done extensive work in modeling hydrodynamic characteristics in planing surface vessels but, as with non-planing craft, a thorough knowledge of the vessel's drag characteristics and the propulsion performance is required. Determining the drag coefficients for the SeaFox ASV would require a long series of tow-testing experiments, or a computer model to be in analyzed using Computational Fluid Dynamics (CFD) software to develop a table of drag coefficient as a function of speed and/or trim angle. A series of field experiments would also be required to completely understand the SeaFox water jet characteristics as well as the interaction between the air and water boundaries within each individual regime. Even if this were done, it is still not possible to develop a mathematical model to represent the vessel's behavior within the transition region, since the vessel cannot remain in transition at steady state.

A second approach is to collect experimental data that plots the ASV's speed as a function of the throttle command. With this approach it is possible to gather data with

numerous throttle changes and, using a System Identification process, develop models that represent all three regimes. The drawback to this approach is that the resulting models are valid only for a given SeaFox loading and only for conditions close to those experienced during the data collection.

It was determined that the model based on experimental data was the most suitable because it allowed modeling of the transition regime and captured the essential nonlinearities and their bounds. This approach also did not require additional equipment and reduced the amount of field experimentation required significantly.

## C. DATA GATHERING

Experimental data was gathered on Lake San Antonio near Paso Robles, CA. Lake San Antonio was selected because it provided the most benign test environment available. During early morning conditions, wind and current had very little effect on SeaFox's speed. These effects were considered negligible and, therefore, minimized the model inaccuracies induced by outside forces.

When using waypoint navigation, SeaFox is programmed to follow straight line paths at a constant velocity, not conduct a series of high-speed maneuvers in succession. Therefore, constant heading trajectories were considered a reasonable approach to data collection. In addition, holding the heading constant ensured that the vehicle speed changes were due primarily to the thrust provided by the water jet combined with the vessel drag. Had turns been executed during these sea trials, turning dynamics would have been coupled with speed dynamics, thereby corrupting the throttle-to-speed relationship.

The SeaFox throttle input is given in terms of throttle percentage. The allowable throttle percentage inputs range from 0% to 99%. When collecting the data, the goals were to capture the vehicle dynamics associated with various step inputs and to determine the crossover points between the displacement, transition, and planing regimes. The following list details the throttle step inputs that were issued to SeaFox during the sea trials.

- From 0% to 99% then 99% to 0%
- From 0% to 99% and back down to 0% in 50% increments
- From 0% to 99% and back down to 0% in 25% increments
- From 0% to 99% and back down to 0% in 10% increments
- When an approximation of the throttle setting at which transition occurs is determined, 1% increments beginning at 5% prior to the expected transition point.

Figure 4 shows a representative sample of data gathered during the field experimentation. The blue line shows the ordered throttle command while the red line shows the vehicles speed. It can be seen that the speed data taken from the GPS unit was quite noisy, especially at higher speeds. This is, in part, due to GPS sensor noise caused by rapid changing of its attitude toward the open sky resulted from interaction between the hull and the water surface. It was noticed that when SeaFox was planing, very little of its hull was in contact with the water; therefore, even though the conditions were relatively calm, any disturbance on the water surface had a much greater effect of the vessel's speed.

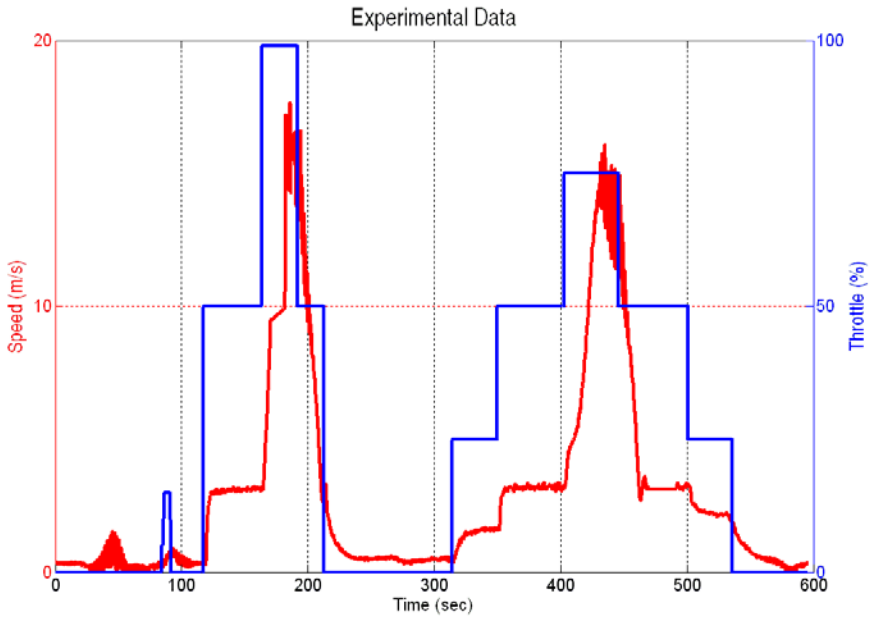


Figure 4. Speed and Throttle Command Data from Field Experimentation

## D. MOTIVATION FOR MODEL STRUCTURE

Initial analysis of the recorded data revealed overshoot behavior in the vehicle's velocity when given a step command, especially in the planing regime. This behavior is indicative of a second order system, therefore the model structure was developed based on the following generic second order linear model [8]:

$$\ddot{x}+2\zeta\omega_n\dot{x}+\omega_n^2 x=0$$

where:

$x$ is the vehicle velocity

$\zeta$ is the damping ratio

$\omega_n$ is the natural frequency

Figure 5 presents the speeds achieved for given throttle commands. The red line represents maximum speed achieved at a specified throttle command during acceleration. The blue line represents the minimum speeds achieved during deceleration. The shaded region represents the variation between the maximum and minimum speeds recorded while planing. It can also be seen that the vehicle speed that correlated to the transition from the displacement regime to the planing regime was different than the speed that correlated with transition from the planing regime to the displacement regime. For this specific set of data, transition from the displacement regime occurred at 4.2 m/s and the vehicle would rapidly increase to 15.5 m/s. When decelerating, transition from the planning regime to the displacement regime would occur at 9 m/s and rapidly decelerate to 3 m/s. Due to this hysteresis it was determined that there would need to be six distinct sub-systems in the model to accurately depict the three operating regimes as well as SeaFox's behavior during acceleration and deceleration. The sub-systems were set up to represent the regimes as follows: Acceleration while in the displacement, transition, or planing regimes, and deceleration while in the displacement, transition, or planing regimes.

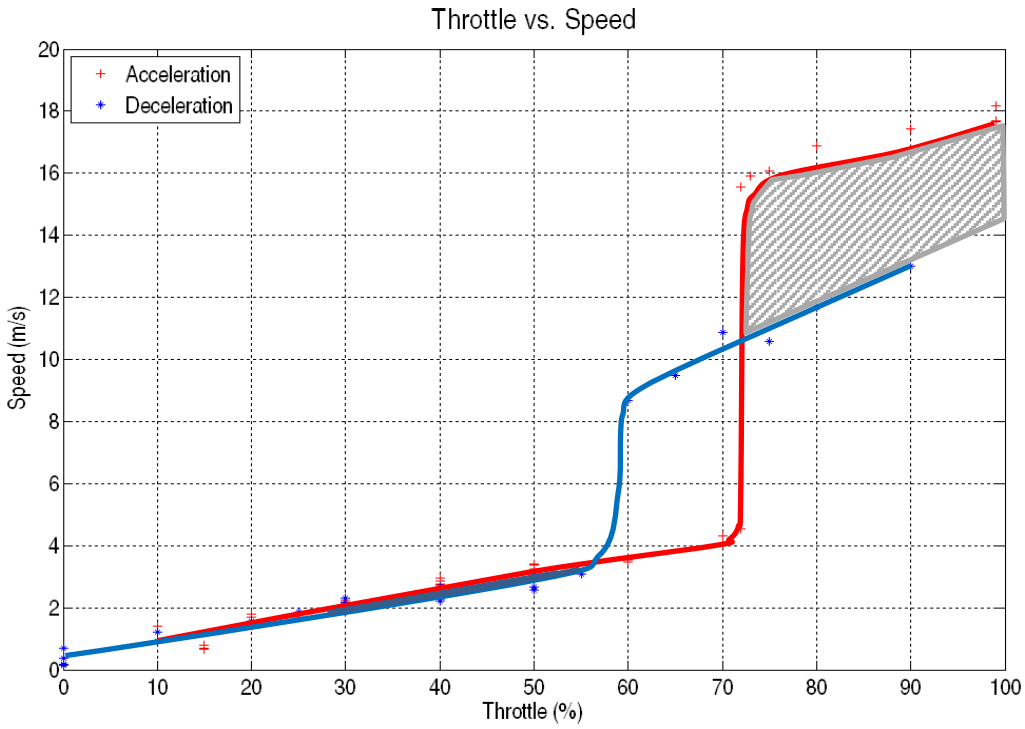


Figure 5. Throttle vs. Speed from Experimental Data Showing Hysteresis

## E. SYSTEM IDENTIFICATION

There are multiple methods in which experimental data can be used to develop a mathematical model [9]. Two processes were used while modeling SeaFox experimental data: 1) the System Identification Toolbox available in MATLAB™ and 2) a process involving the *fminsearch* function within the MATLAB environment. Using two methods provided a means of comparing and validating the results of the System Identification process. If both methods produce matching results then the parameters can be regarded as reasonable and trustworthy estimates of the actual parameters.

Prior to developing the models, the experimental data needed to be processed to remove outliers. The data was pre-processed using MATLAB's embedded Curve Fitting Toolbox. The Loess method used creates a smooth data set through linear least-squares fitting with a second degree polynomial [10]. This process was completed for all of the data sets that appeared to be free of outliers and that were collected from sea trials that were 20 seconds or longer in duration.

The MATLAB embedded System Identification Toolbox is designed to develop a best-fit, user defined model from experimental data sets. The process in which the plant parameters were developed are outlined in [11]. After all of the data sets were pre-processed they were imported into the System Identification Toolbox. Because it was desired to create a second order linear model to represent each regime, the Process Model option was chosen. To develop the correct structure of the transfer function, the process model was set to develop a model of an under-damped system with two poles and a delay. This would produce the parameters of the transfer function:

$$G(s)=\frac{Ke^{-T_d s}\omega_n^2}{s^2+2\zeta\omega_n s+\omega_n^2}$$

where:

K is the DC gain

$T_d$ is the time delay in the system

$\zeta$ is the damping ratio

$\omega_n$ is the natural frequency

Figure 6 shows the setup of the Process Models GUI. After the toolbox completed the estimation of the model parameters, the values of K, $\zeta$, $\omega_n$, and the fit percentage were recorded for later comparison. The fit percentage was based on the following equation:

$$\text{Fit \%} = \left[1-\frac{\text{norm}(y-\hat{y})}{\text{norm}(y-\text{mean}(y))}\right]*100$$

where y is the measured output and $\hat{y}$ is the simulated model output as outlined in [11] . This process was completed for all valid data sets that did not transition out of their original regime. Results from this analysis are provided in Appendix A, Tables 1 through 4.

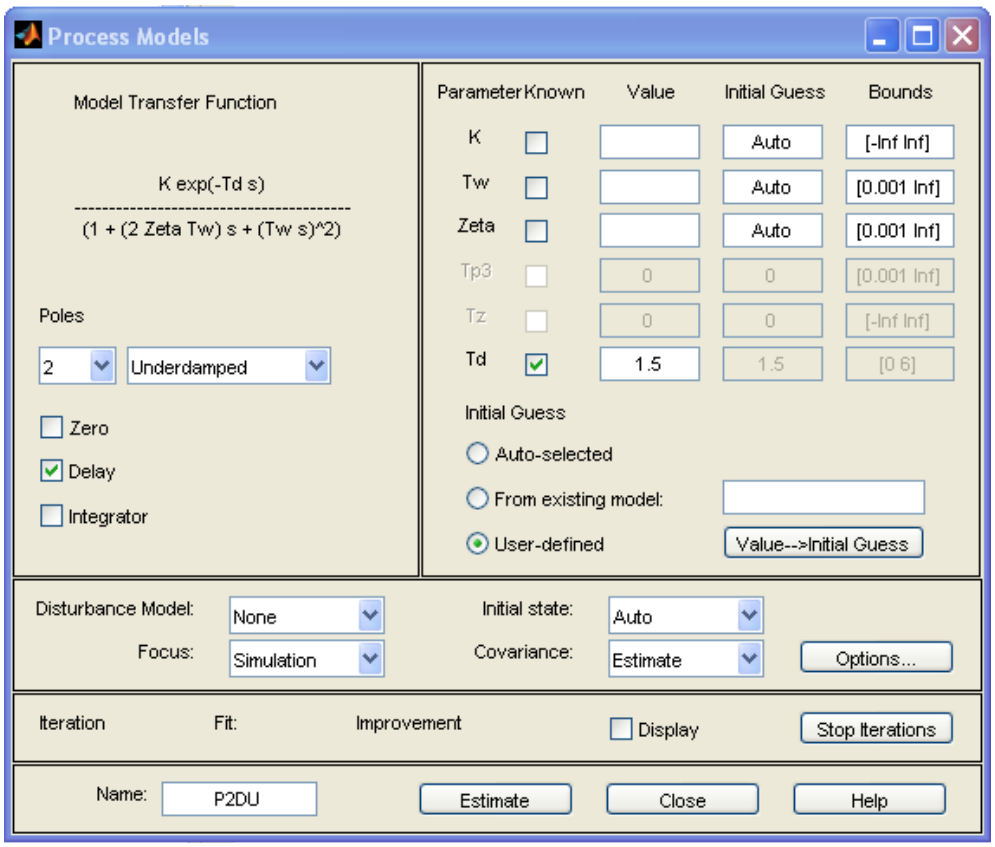


Figure 6. Process Models GUI

The second method for determining the transfer function variables utilized the *fminsearch* function as demonstrated in [11]. In this method, a model shown in Figure 7 was used to determine the error between the actual data and simulated system response given values of K, $\zeta$, and $\omega_n$. Figure 7 represents a second order model developed in Simulink with the input being the recorded throttle commands from the experimental data and the output being error between experimental data speed and the speed produced from the model. The total error was compared to a set tolerance and then, using a Nelder-Mead simplex algorithm, the *fminsearch* function modified the parameters for the next iteration [12]. This process was continued until the square of the errors was within 0.01 of the actual data. When the process was completed, the values of K, $\zeta$, and $\omega_n$ were recorded for later comparison. Results from this analysis are provided in Appendix A, Tables 5 through 8.

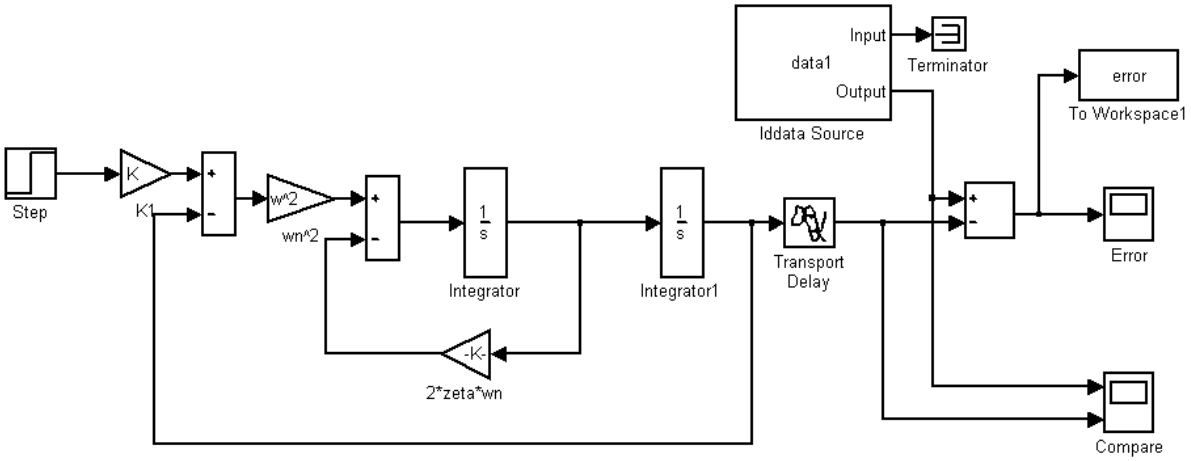


Figure 7. *fminsearch* Parameter Estimation Model

Data sets in which the ASV's speed remained in either the displacement or planing regime were used when determining the model parameters using either the System Identification or the *fminsearch* method. This allowed modeling the vehicle's characteristics outside of the transition regime. Once values of K, $\zeta$, and $\omega_n$ were determined for the displacement and planing regimes using both methods, it was observed that within the individual regimes, there was very little deviation between the System Identification results and the *fminsearch* results. The parameter values for each region were then averaged to develop a set of values that best modeled the average plant characteristics.

Mathematical modeling of the transition region is difficult due to the inability to manually maintain SeaFox's speed within this region as well as the inability to isolate data from the trial runs that was solely in the transition region. To model the transition regions, it was necessary to interpolate parameter values from models of the planing and displacement regions, as well as data sets which included transitions between all regions.

After model parameters were determined for all three regimes in acceleration and deceleration, a final model was developed to simultaneously incorporate each of the six sub-models. Logic was implemented to select the appropriate regime sub-model based on the current speed and throttle commands.

A time delay of approximately 1.5 seconds, between throttle command and speed response, was noticed during the data gathering and system identification processes. This delay represented the processing time of the signal as well as the actuating time of the engine components and it was consistent throughout all of the operating regions. To account for this in the Simulink model of SeaFox, a Transport Delay block was inserted in the command input signal. Figures 8 and 9 show examples of the simulated model response compared to actual SeaFox data. More comparisons can be seen in Appendix B. Figure 10 shows the complete Simulink model representing SeaFox's throttle vs. speed dynamics. The blue subsystems represent the displacement, transition, and planing regimes when accelerating while the yellow represent the three regimes when decelerating. The green section represents the logic process that determines which regime, or subsystem, represents the current ASV dynamics. The input to the model are actual throttle commands from experimental data while the output is the speed determined from the model and the error between the model output and the experimental data.

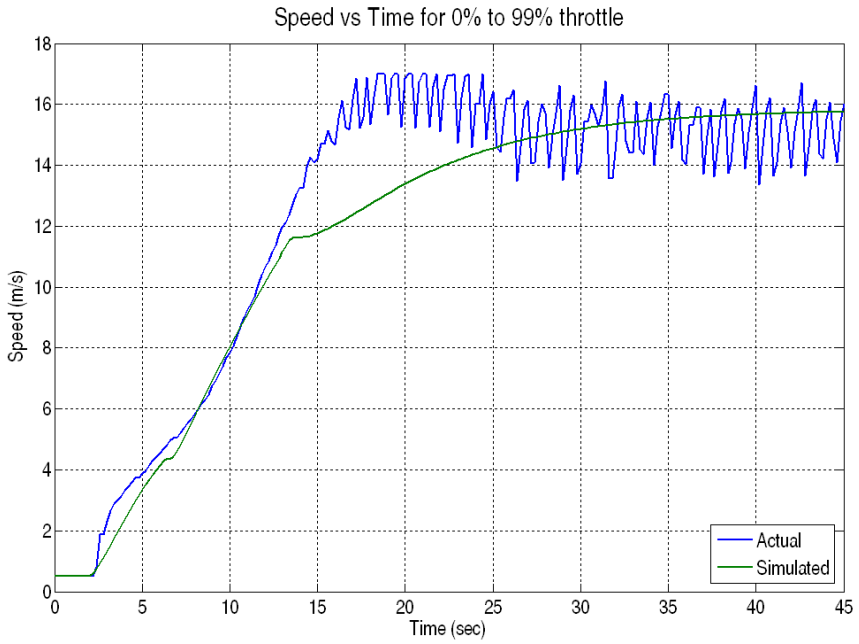


Figure 8. Model Comparison with Actual Data for a 0% to 99% Throttle Change

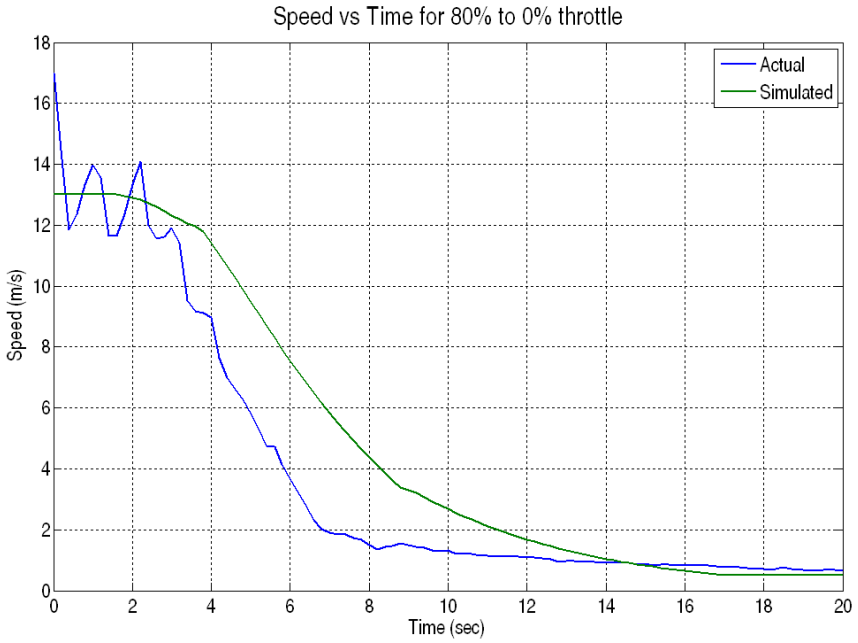


Figure 9. Model Comparison with Actual Data for a 85% to 0% Throttle Change

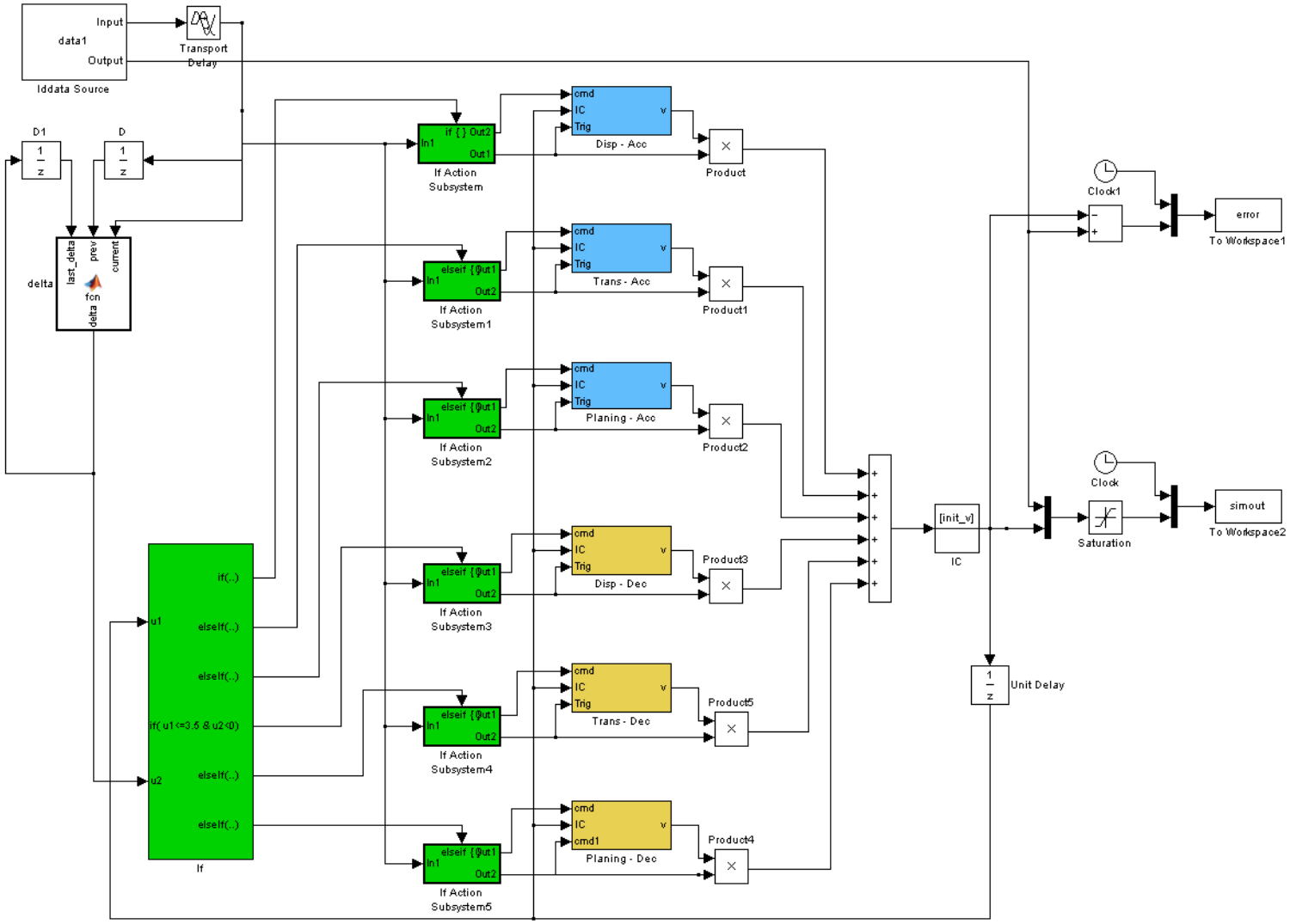


Figure 10. SeaFox Throttle Dynamics Model

THIS PAGE INTENTIONALLY LEFT BLANK

# III. CONTROLLER DESIGN

## A. CHAPTER OVERVIEW

This chapter addresses the design of three control algorithms representing qualitatively different control architectures; they include (i) PID, (ii) MRAC, and (iii) $\mathcal{L}_1$ controllers. On one hand, they represent the increasing complexity of control architectures in an attempt to address the nonlinear nature of the control problem. On the other hand they demonstrate the achievable controller structure, as well as the required tradeoffs. Each controller is integrated with the SeaFox model discussed in Chapter II and can be simulated with and without realistic operational disturbances. This provides a basis for objective comparison among the controllers and gives a means to show relative robustness and performance in the challenging operational conditions. Comparisons are performed with simulated reference commands in the displacement, transition, and planing regions.

## B. PID CONTROLLER WITH GAIN SCHEDULING

The first controller to be implemented using the SeaFox model is the Proportional-Integral-Derivative (PID) controller. The results using the PID controller will be the performance baseline to which the results of the MRAC and the $\mathcal{L}_1$ controller will be compared. PID controllers are some of the most widely used industrial controllers in marine and aerospace engineering. This is due to their simplicity and robustness in the presence of limited disturbances. The PID controller takes into account the current error, the accumulation of past errors, and the rate of change of the error as described in [13]. Figure 11 illustrates a basic PID controller. The mathematical expression for the ideal PID controller can be expressed as follows:

$$U(s) = G_c(s)E(s)$$

with

$$G_c(s) = K_p\left(1 + \frac{K_i}{s} + K_d\frac{N}{1 + N\frac{1}{s}}\right)$$

where:

E is the error between the reference command and the plant output

$K_p$ is the proportional gain

$K_i$ is the integral gain

$K_d$ is the derivative gain

N is the filter coefficient for the derivative approximation

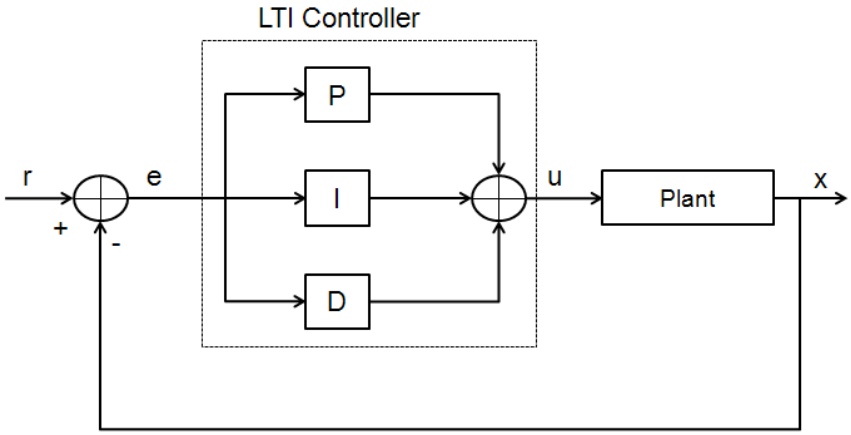


Figure 11. Basic PID Controller Block Diagram (From Åström and Hägglund, 1995)

The problem faced when attempting to use a PID controller onboard SeaFox is that it is a linear controller with constant parameters with no explicit knowledge of the plant varying dynamics. Because the hydrodynamic properties change as SeaFox transitions through the speed regimes, it creates significant nonlinearities within the plant. To compensate for the nonlinearities, a simple gain scheduling approach can be incorporated to account for the varying plant parameters. The gain scheduling is implemented so that as the ASV transitions between the displacement and planing regimes, the values of $K_p$, $K_d$, $K_i$, and N are adjusted to adapt to the new plant parameters. Astrom [14] states that "an adaptive controller is a controller with adjustable parameters and a mechanism for adjusting the parameters." By this definition, addition of the gain scheduler converts the standard PID controller into the simplest variant of an adaptive controller.

Because the SeaFox has upper and lower bounds on the control signal, integrator windup becomes an issue that must be accounted for. When the control signal reaches the limits of the actuator, the feedback loop becomes broken. At this point, the integrator will continue to integrate the error and possibly create a very large output. This would require an error signal of the opposite sign to be exhibited for a long period of time in order to counteract this "wind up." One method to account for windup is through back-calculation as outlined in [13]. Back-calculation determines the difference in the control signal and the saturation limits and then feeds this error through a gain then back to the integrator. This creates a feedback path around the integrator which causes the control signal to stabilize at the saturation limit and allows it to react as soon as the error signal changes sign.

A problem in using a pure derivative term is that the output is proportional to the rate of change of the input error signal. Since there is always some noise associated with the sensors, this can produce noisy changes in the error signal. This would lead to unnecessary and extreme actuator movement and equipment damage. To counter this negative effect, the pure derivative term has been replaced with a derivative filtering scheme. The design of the PID controller with the anti-windup feature and derivative filtering scheme can be seen in Figure 12. This model represents the controller as a function the scheduled gains and the error between the plant output and the reference values.

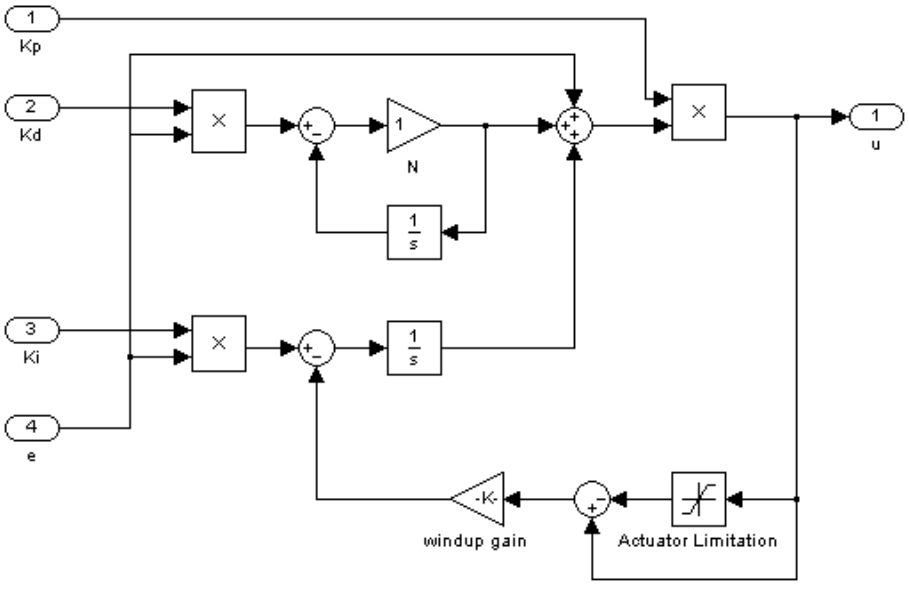


Figure 12. PID Controller with Anti-Windup and Derivative Filtering

A low-pass filter is implemented to attenuate high frequency control signals and limit the rate at which the control signal may vary. This has been done to smooth the transitions between control commands and to avoid damaging the SeaFox mechanical equipment due to large, rapidly varying commands. A complete model of the PID controller implementation can be seen in Figure 13. This diagram shows the overall relationship between the reference command, plant output, controller, gain scheduler, pre-filter, and throttle control limiter.

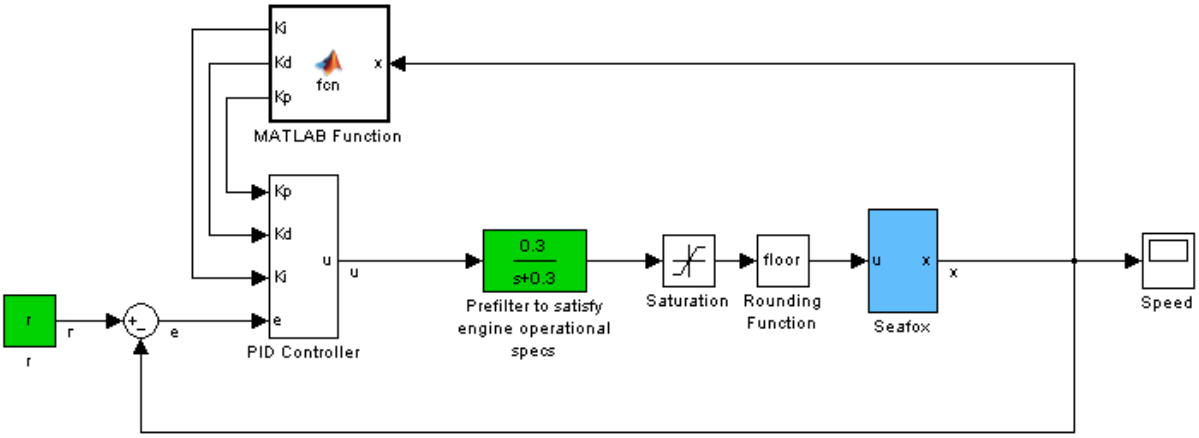


Figure 13. System Diagram with PID Controller combined with Gain Scheduling and Low-Pass Filter

In [13], there are several methods available for tuning PID controllers, including manual (Ziegler-Nichols method) and automatic tuning methods which can be chosen based on user preference. A version of automatic tuning was used to tune the SeaFox PID controller. An *fminsearch* script similar to that in Appendix C was used to minimize the overshoot and settling time allowed by the controller. This procedure was performed with a low-speed reference signal to determine the gain values for the displacement regime. This process was repeated with a high-speed reference signal to determine the gain values for the planing regime. This process was validated using a Ziegler-Nichols method combined with engineering intuition[13]. The tuned parameters are listed in Appendix D.

## C. COMPOSITE MRAC WITH INPUT CONSTRAINTS AND GAIN SCHEDULING

The MRAC was the first variant of adaptive control architecture to be developed for the SeaFox ASV. The MRAC was chosen due to the following advantages over linear control designs:

- Guaranteed asymptotic stability
- Robust performance in the presence of bounded disturbances
- The ability to define the desired plant behavioral characteristics through the use of a reference model
- Detailed knowledge of the actual plant parameters is not required

By utilizing the composite MRAC scheme, the transient characteristics obtained will be improved over the conventional MRAC by utilizing prediction and tracking errors.

Ioannou and Fidan[15] state that a Model-Reference Adaptive Control (MRAC) is typically composed of four parts: a plant, a reference model, a controller, and an adaptive law. The relationship between these components can be seen in Figure 14. The plant that the MRAC is designed to control usually has a known structure but some or all of the plant parameters may be unknown. This type of controller is useful for plants such as SeaFox, which exhibit second order speed behavior, but have unknown parameters that vary with speed and environmental factors.

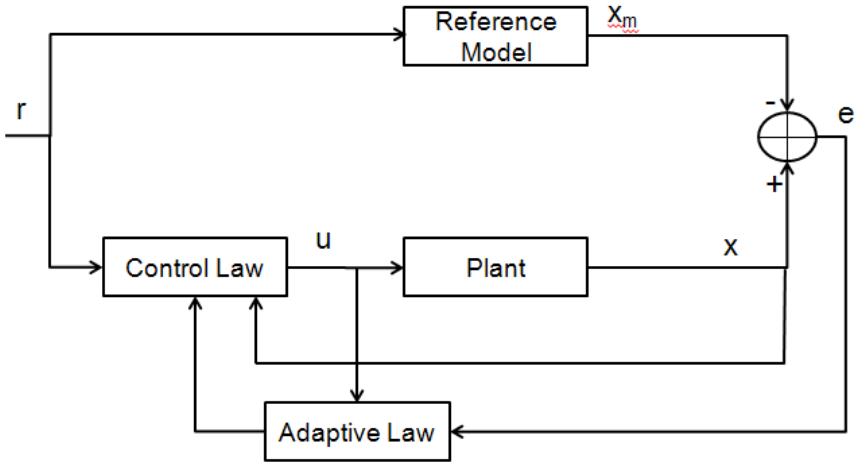


Figure 14. Block Diagram of a Model Reference Adaptive Control (From Ioannou and Fidan, 2006)

The reference model is used to define the ideal plant response. The design of the reference model must take into account the desired performance of the plant and must have characteristics which are achievable; these reasonable bounds were identified during the system identification process. A relatively non-aggressive first-order model was used in designing the MRAC for the SeaFox. The desired outcome from using a first-order reference model was to minimize the amount of overshoot displayed by the ASV, while keeping the rise time within a feasible range. The goal was to limit the overshoot to 10% and to maintain the rise time under one minute for any step command. The reference model is expressed by the following equation:

$$\dot{x}_m(t) = a_m x_m(t) + b_m r(t),\ a_m < 0,\ x_m(0) = x_0$$

where

MRAC adaptation laws through the use of state predictors as described in [16]. The state predictors produce an estimate of the plant output at the next time step for use in the control law in order to improve performance. The composite adaptive law is represented by the following set of equations:

$$
\begin{aligned}
&u(t) = k_x(t)x(t) + k_r(t)r(t) \\
&\dot{k}_x(t) = -\gamma_x x(t)(e(t) - \gamma\tilde{x}(t))\,\mathrm{sgn}(b),\ k_x(0) = k_{x0} \\
&\dot{k}_r(t) = -\gamma_r r(t)(e(t) - \gamma\tilde{x}(t))\,\mathrm{sgn}(b),\ k_r(0) = k_{r0} \\
&e(t) = x(t) - x_m(t)
\end{aligned}
$$

where $u$ is the controller command, $k_x$ and $k_r$ are the adaptive gains, $\gamma$, $\gamma_x$ and $\gamma_r$ are the adaptation gains and $x(t)$ is the state output of the plant. The state predictor is represented by the following equation:

$$\dot{\hat{x}}(t) = a_p\tilde{x}(t) + a_m x(t) + b_m r(t),\ \hat{x}(0) = x_0$$

where $\hat{x}$ is the predicted state output and $\tilde{x}$ is the prediction error. By choosing $|a_p| > |a_m|$ the prediction error dynamics will converge to zero much faster than the tracking error dynamics, thereby improving the adaptation rates of the system.

SeaFox is also limited in the range of available throttle commands. Although it is possible to command negative throttle commands to induce reverse motion but for the sake of keeping the system model of reasonable complexity the throttle command range was limited by [0% , 99%]. Since the input command to the system is constrained, the tracking error dynamics between the reference model and the plant become unbounded. The constraint on the control input can be seen as:

$$u(t) = \begin{cases} u_c(t), & |u_c(t)| \le u_{\max} \\ u_{\max}\,\mathrm{sgn}(u_c(t)), & |u_c(t)| > u_{\max} \end{cases}$$

where $u_c$ is the commanded control input and $u_{\max}$ is the maximum control input allowed by the system.

With the above constraint the reference model becomes:

$$\dot{x}_m(t) = a_m x_m(t) + b_m(r(t) + k_u\Delta u(t))$$

where $\Delta u = u(t) - u_c(t)$ and $k_u$ is an additional adaptive gain. The new adaptation law is:

$$\dot{k}_u(t) = \gamma_u \Delta u(t)(e(t) - \gamma \tilde{x}(t))b_m$$

with $\gamma_u$ being a new adaptation gain. There is an extensive body of research addressing stability of numerous variations of MRAC. Proofs of their stability can be found in [16], [17].

Although MRAC design techniques can develop controllers for systems with unknown parameters, these techniques are developed to achieve the desired performance assuming that those parameters are constant. As it was discussed in the previous chapter, SeaFox has three speed regimes with very distinct parameters. Therefore, to account for variation of control parameters in each speed regime, gain scheduling was once again utilized to adjust the values of $a_p$, $\gamma$, $\gamma_x$, $\gamma_r$ and $\gamma_u$. This illustrates one of the drawbacks of using MRAC; even though MRAC can accommodate unknown plant parameters, some knowledge or physical insight into the plant dynamics is required to properly develop and tune the controller.

In control architectures such as the MRAC, parameter drift becomes a concern for the system stability. Parameter drift usually occurs when there are small tracking errors between $x$ and $x_m$. While the tracking errors might remain small, the errors between the estimated plant parameters and the actual plant parameters may grow, causing an increase in control effort and eventually leading to instability of the system. There are multiple methods which counter the negative effects of parameter drift such as using projection based operators, $\sigma$-modification or $e$-modification[15]. In the case of the MRAC implemented onboard SeaFox, a modification of the projection operator technique that limits the integrator outputs of $k_x$, $k_r$, and $k_u$ was utilized. This enabled keeping the parameters bounded to maintain stability. The full implementation of the composite MRAC with input constraints can be seen in Figures 15 through 18.

There are no standard predefined tuning methods for determining the gains in a MRAC system. Again, practical implementation and tuning still relies heavily on a designers' knowledge of the system and the operational conditions. The tuning process used

for the SeaFox design consisted of an iterative tuning in which the gains were adjusted based on the objective measurements and in part on engineering intuition. The tuned controller parameters are listed in Table 10 in Appendix D.

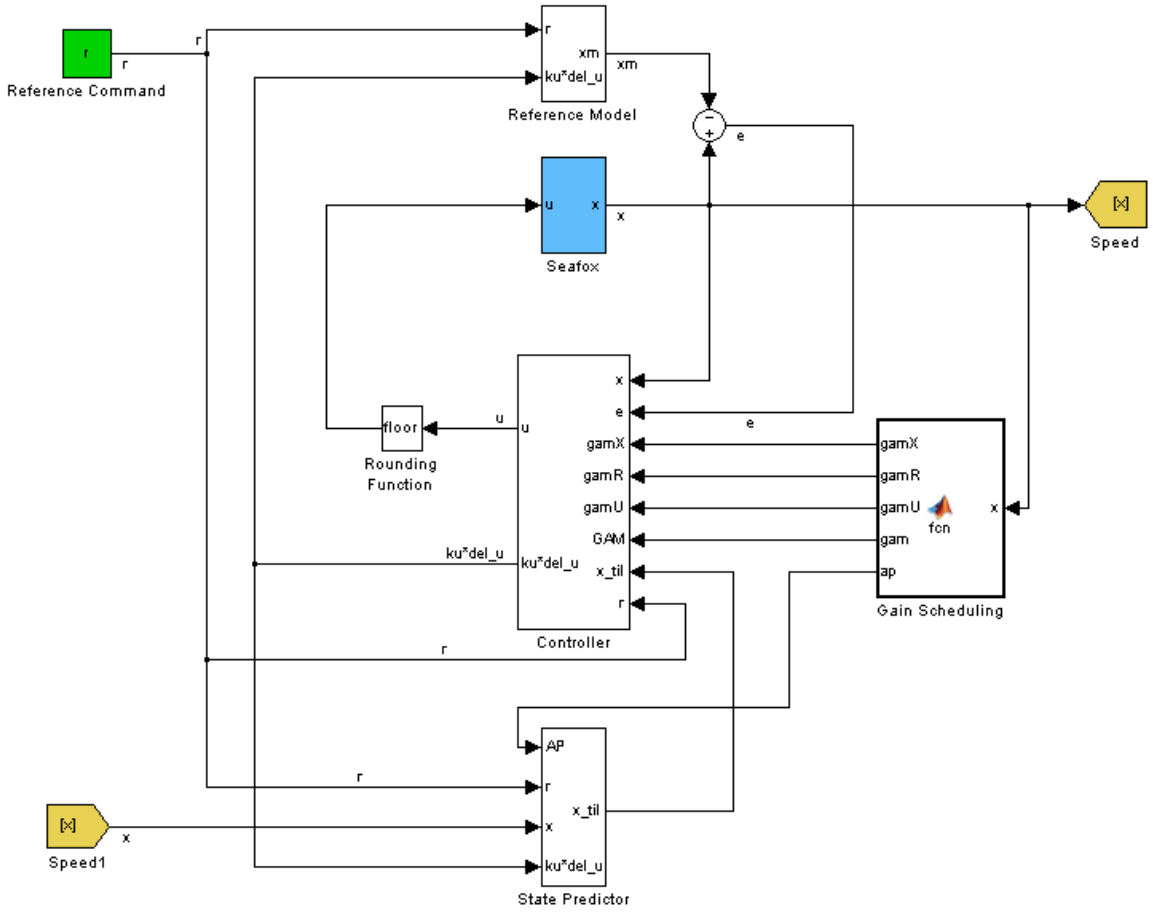


Figure 15. Composite MRAC

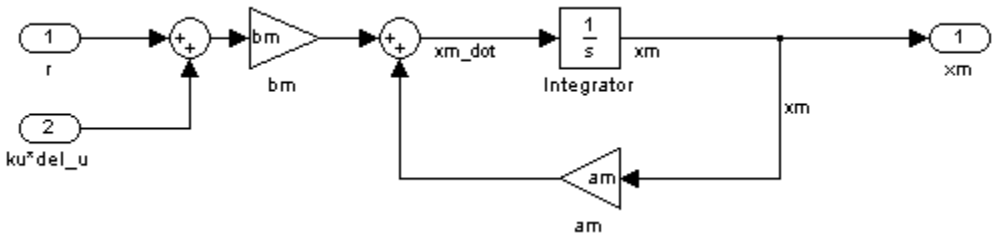


Figure 16. Composite MRAC Reference Model

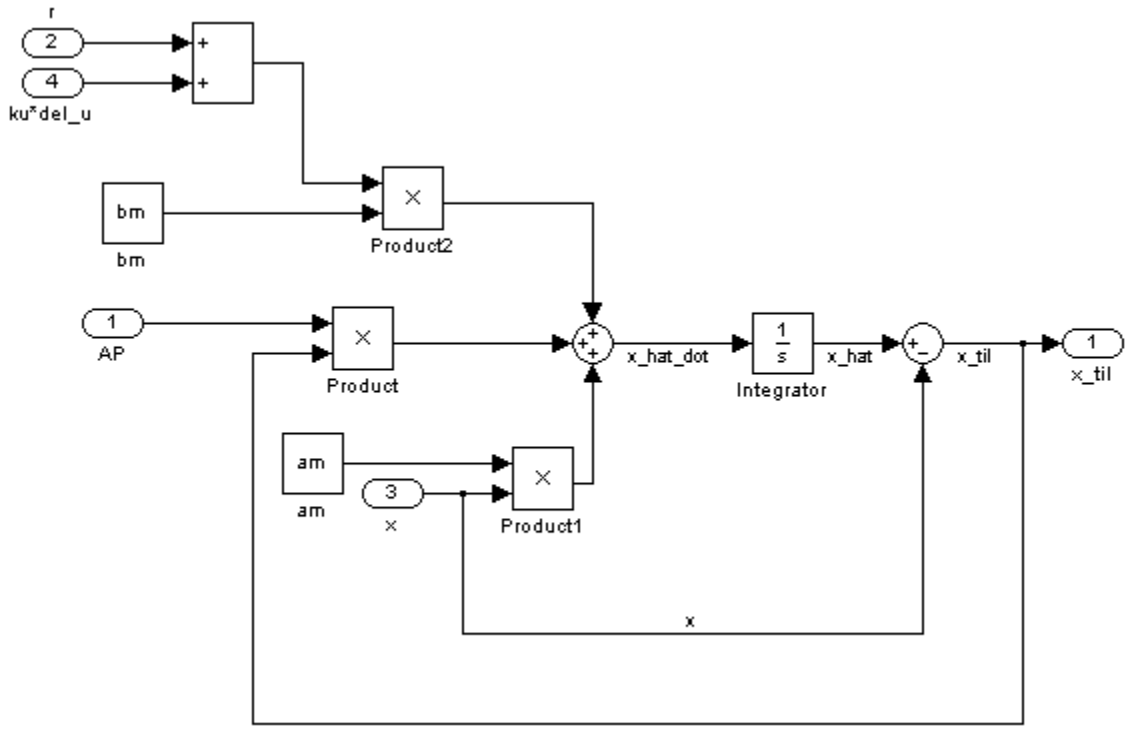


Figure 17. Composite MRAC State Predictor

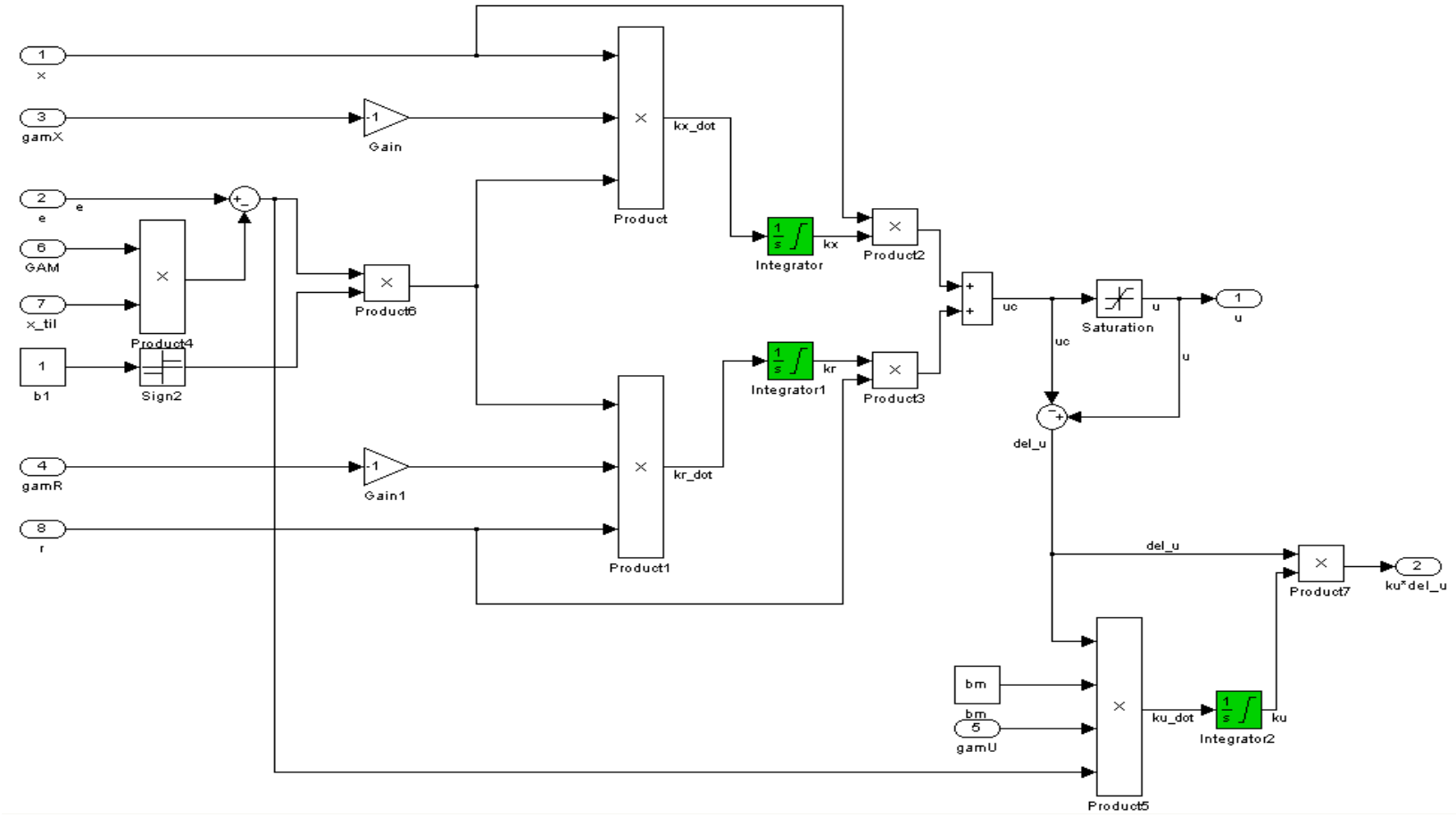


Figure 18. Composite MRAC Adaptive Law and Controller

## D. $L_1$ CONTROLLER

The $L_1$ control architecture is a relatively new method in the field of adaptive control. The key difference and the goal of the $L_1$ adaptive control is to decouple the adaptation rate from the robustness properties. The architecture of the $L_1$ controller differs from that of the MRAC such that with the MRAC, the adaptation rate and robustness are closely coupled, forcing a design trade-off; if a fast adaptation rate is desired, stability margins suffer. From [18], the advantages of $L_1$ adaptive control theory are as follows:

- Guaranteed robustness in the presence combined with fast adaptation
- Separation of adaptation and robustness
- Guaranteed transient response.
- Guaranteed time-delay margin.
- Uniform scaled transient response dependent on changes in initial conditions, unknown parameters, and reference inputs.

The design of the $L_1$ controller for the SeaFox is based on the pioneering work of Dr. Naira Hovakimyan who has done extensive development and analysis on the $L_1$ controller and its properties. The implementation of the $L_1$ controller follows the architecture presented in [18–20]. A block diagram of the $L_1$ control structure is shown in Figure 19 as a reference in the following discussion.

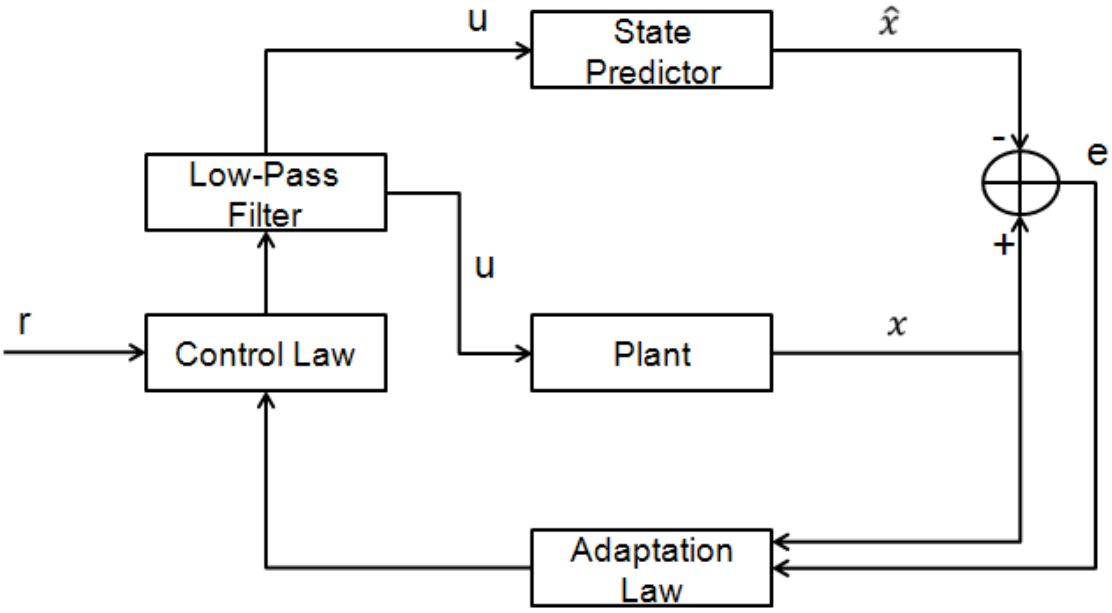


Figure 19. $L_1$ Adaptive Controller Block Diagram (From Hovakimyan and Cao, 2010a)

As with other methods of adaptive control, the $L_1$ controller is designed to develop a control signal for a system with unknown parameters and bounded disturbances. Unlike the MRAC approach described above, the values of the plant parameters, although unknown, are allowed to be time-varying. This is a major advantage of the $L_1$ architecture over the MRAC architecture because it eliminates the need for gain scheduling.

From Figure 19 it can be seen that the $L_1$ controller structure is somewhat similar to that of the MRAC, however the reference model is not an explicit part of the $L_1$ controller. Instead, the reference model is accounted for in the design of the state predictor. Also, the $L_1$ controller has a low-pass filter in the control signal, whereas the MRAC architecture does not.

The low-pass filter and the state predictor are instrumental in decoupling the adaptation rate and robustness. This decoupling allows a designer to tune robustness properties via the parameters of the low-pass filter, while separately increase the adaptation rate via the adaptation gains.

The chosen filter parameters, which determine the filter bandwidth, directly affect the performance and the stability of the system. The $L_1$ controller proofs of stability use the $L_1$ norm of a cascaded system for determining the filter parameter requirements. This is how the $L_1$ controller gets its name. By using the small gain theorem and the induced $L_1$ norm through the $L_\infty$ norm of the inputs and outputs, the performance of the system can be determined to be bounded and stable [18].

Using the approach of the $L_1$ theory, the following state predictor was used:

$$\dot{\hat{x}}(t) = A_m \hat{x}(t) + b\hat{v}(t),\ \hat{x}(0) = \hat{x}_0$$
$$\hat{v}(t) = \hat{\omega}(t)u(t) + \hat{\theta}^T(t)x(t) + \hat{\sigma}(t)$$

where $\hat{\omega}(t)$, $\hat{\theta}(t)$, and $\hat{\sigma}(t)$ are based on the following adaptation laws:

$$\dot{\hat{\theta}}(t) = \Gamma \mathrm{Proj}(-x(t)\tilde{x}^T Pb, \hat{\theta}(t)),\ \hat{\theta}(0) = \hat{\theta}_0$$
$$\dot{\hat{\sigma}}(t) = \Gamma \mathrm{Proj}(-\tilde{x}(t)Pb, \hat{\sigma}(t)),\ \hat{\sigma}(0) = \hat{\sigma}_0$$
$$\dot{\hat{\omega}}(t) = \Gamma \mathrm{Proj}(-\tilde{x}(t)Pbu(t), \hat{\omega}(t)),\ \hat{\omega}(0) = \hat{\omega}_0$$

where $\tilde{x}(t) = \hat{x}(t) - x(t)$ is the estimation error, $\Gamma > 0$ is the adaptation gain, *Proj()* is the projection operator, and $P$ is the solution to the Lyapunov equation $A_m{}^T P + PA_m = -Q$. For the purpose of the SeaFox controller design, $Q$ was initially chosen to be identity. The control signal is determined by:

$$u(s) = -k\chi(s)$$
$$\chi(s) = D(s)(\hat{v}(s) - k_g r(s))$$

where $k>0$, $kg = -1/(c^T A_m{}^{-1} b)$, and $D(s)$ is a transfer function that leads to a stable $C(s) = \omega k D(s)/(1 + \omega k D(s))$. Stability proofs can be found in [20]. Implementation of the control structure can be seen in Figures 20 through 22.

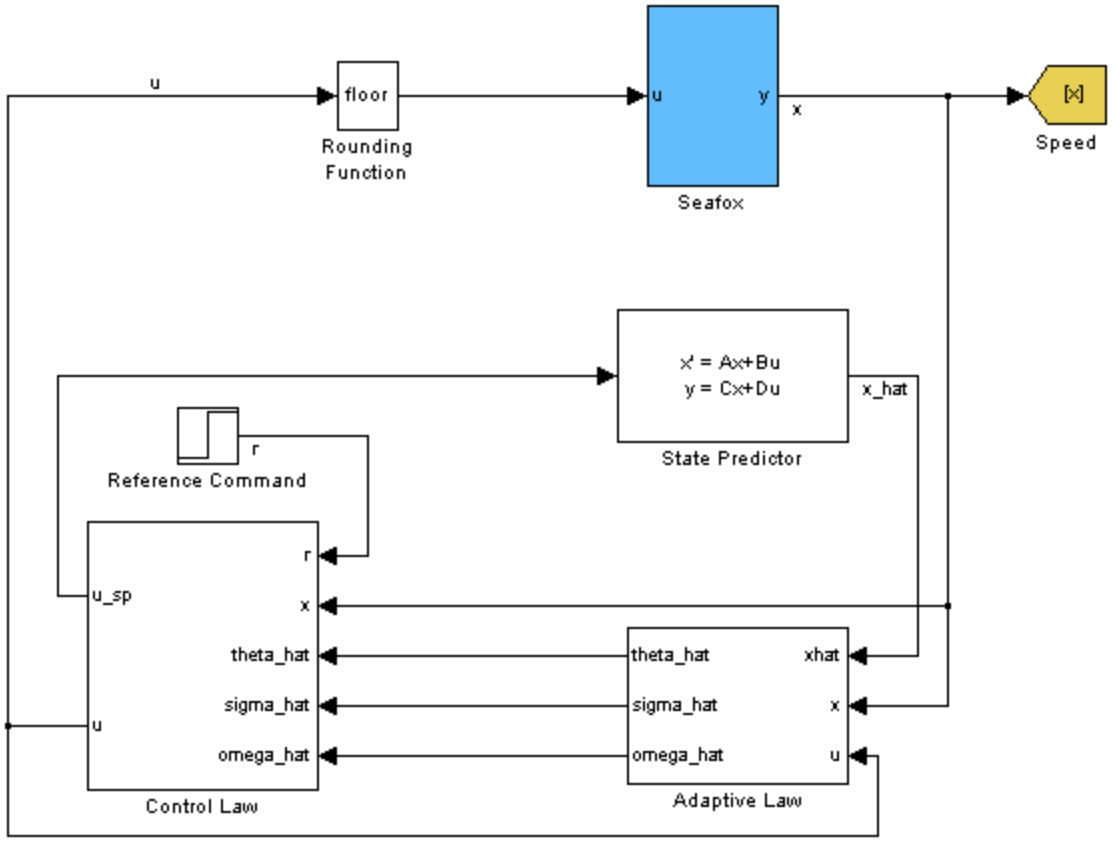


Figure 20. $L_1$ Adaptive Controller

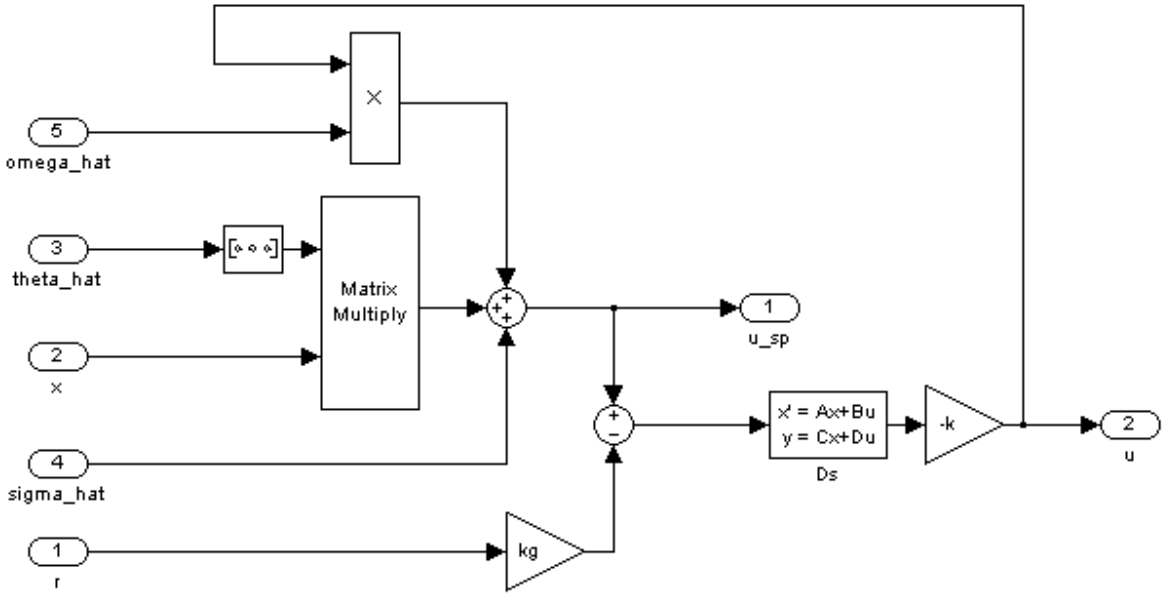


Figure 21. $L_1$ Control Law

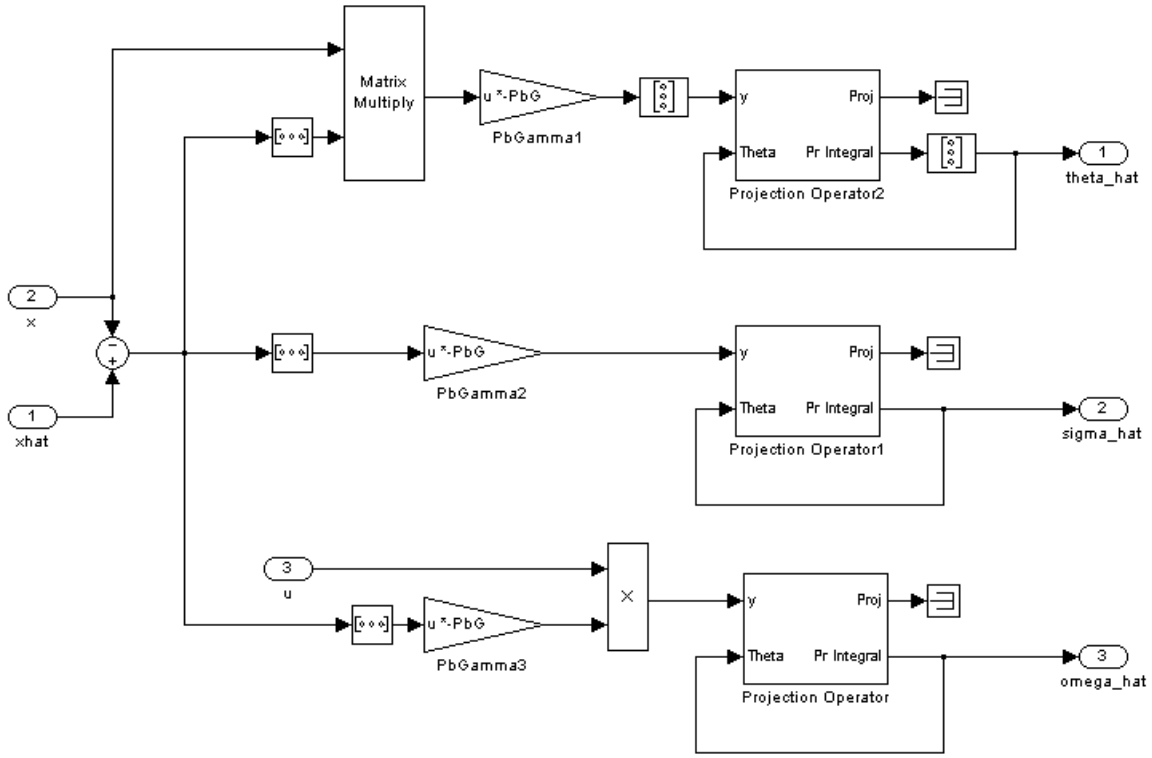


Figure 22. $L_1$ Adaptive Law

As with the MRAC, there is no standard tuning procedure for the $L_1$ controller. The controller tuning relied on an iterative process and engineering intuition to determine the parameter values. This tuning process determined values of $\Gamma$ and $A_m$, the transfer function $D(s)$, and the bounds for $\hat{\omega}$, $\hat{\sigma}$, and $\hat{\theta}$. Their numerical values can be found in Appendix D.

# IV. SIMULATION AND SEA TRIAL RESULTS

## A. CHAPTER OVERVIEW

This chapter presents a comparative analysis of the performance of the PID, MRAC, and $L_1$ controllers. Each controller is compared based on their speed tracking performance and control effort for a given reference command within each of the three regimes. This chapter also compares the performance of the PID and the MRAC controllers during sea trials on Monterey Bay.

## B. SIMULATION RESULTS

During the simulation phase, the PID, MRAC, and $L_1$ controllers were analyzed in the Simulink environment to compare their relative ability to accurately track a reference command with minimal control effort. Most controllers can be tuned so that there is minimal error between the reference command and the plant output but in most cases this requires increased control effort. For ASV's such as SeaFox, this can be a detrimental effect because an aggressive control effort can lead to an increased probability of engine failure and higher maintenance costs. The goal in tuning the controllers for SeaFox was to minimize tracking error while maintaining control effort at a minimum to reduce the risk of excessive wear on the mechanical equipment.

In each simulation the system was subject to three conditions: no disturbances, a constant disturbance, and an oscillatory disturbance. The case without a disturbance represents benign conditions similar to those found on a lake on a calm day. The case with a constant disturbance represents a steady headwind or current. The oscillatory disturbance represents operations in rough seas with large swells.

### 1. Displacement Regime Results

Figure 23 shows the system responses when given reference commands of 3 m/s without disturbances. All three controllers exhibit acceptable responses. The $L_1$ controller has the smallest rise time and exhibits very minor oscillations. Figure 24 shows the controller command signal for the same scenario. Again, all three controllers

exhibit acceptable behavior in that they all have smooth control signals. The $L_1$ does have a slight overshoot but this is due to the aggressiveness of the controller. The small oscillations of the L1 controller are shown here to illustrate the tradeoff between the fastest rise time (performance) and robustness. Attenuating these oscillations is straightforward but will result in longer rise time. It also important to note that the controller processing speed is much higher than throttle controller's ability to accept commands. Therefore, the small, high frequency oscillations will be attenuated by the throttle controller.

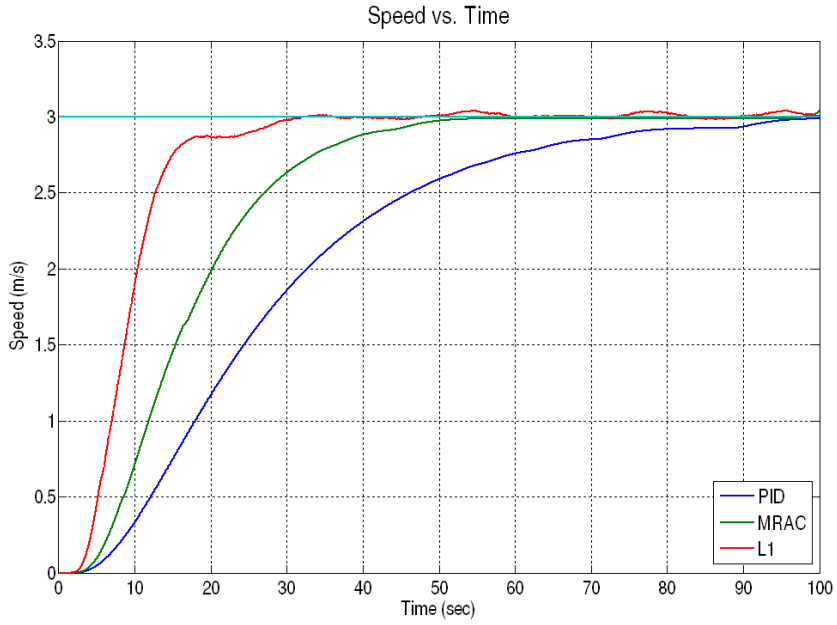


Figure 23. System Response: 3 m/s Reference Command, No Disturbance

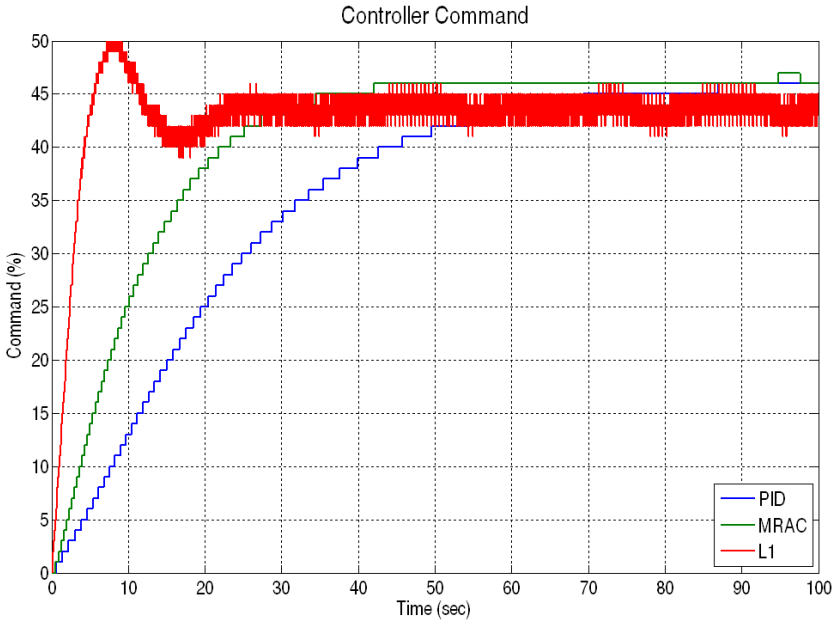


Figure 24. Controller Response: 3 m/s Reference Command, No Disturbance

Figure 25 shows the system responses for a given reference commands of 3 m/s with a constant 3 m/s disturbance. All three of the controllers exhibit an over-shoot in the initial response but the adaptive controllers compensate very quickly and converge to the commanded speed with only slight oscillations about the reference signal. The PID controller, again, has the slowest response time and has difficulty tracking the reference command. It exhibits much larger oscillations about the reference command compared to the MRAC and $L_1$ controllers.

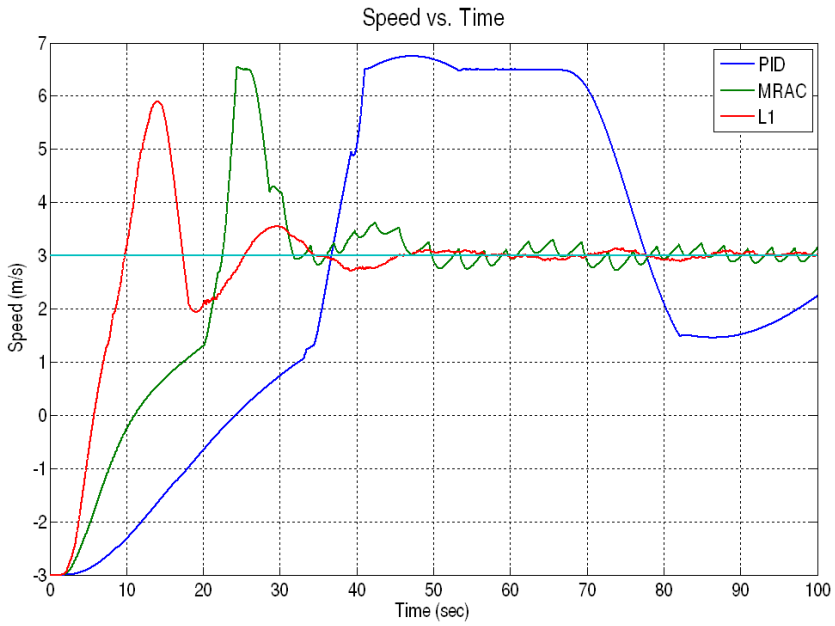


Figure 25. System Response: 3 m/s Reference Command, Constant Disturbance

Figure 26 shows the controller command signal for the same scenario. The adaptive controllers are obviously significantly more aggressive in tracking the reference command as shown by initial command signal and the small oscillations in steady state. Even though this requires more control action than the smooth control signal of the PID controller, it is an acceptable tradeoff for the improved performance.

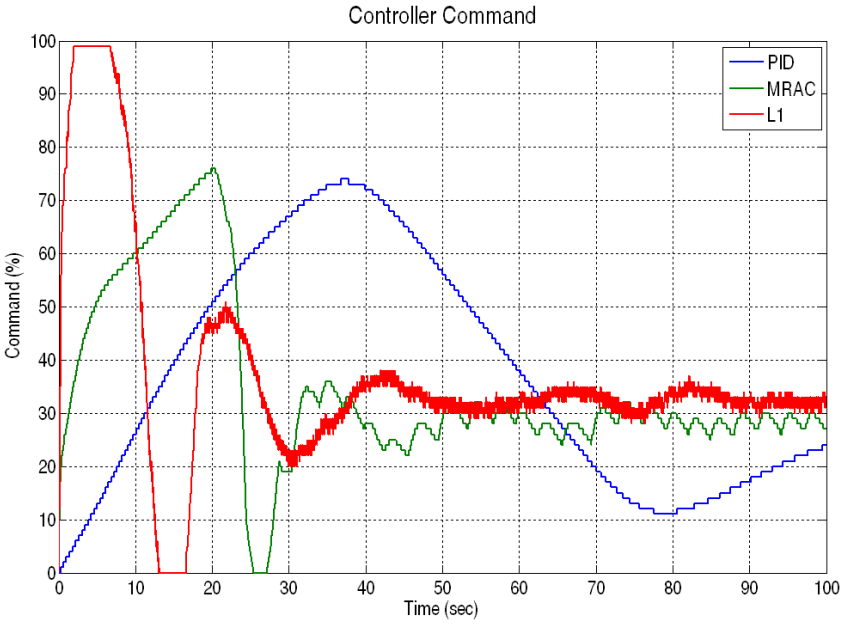


Figure 26. Controller Response: 3 m/s Reference Command, Constant Disturbance

Figure 27 shows the system responses for a given reference commands of 3 m/s with a sinusoidal disturbance having a peak amplitude of 2 m/s and a frequency of 0.1 rad/sec. This disturbance approximates operations in rough seas, particularly when the ASV travels up the face of a swell and then down the back side. The PID controller has the most difficulty compensating for this disturbance. It can be seen that the ASV's speed oscillates about the reference command with a frequency close to that of the disturbance but with peak errors greater than that of the peak disturbance value. The MRAC oscillates as well. However, with the exception of a spike at approximately 58 seconds, it achieves a smaller peak error value than the PID controller. It is believed that the spike exhibited by MRAC is due to inaccuracies in the model behavior and not due to the controller itself. The $L_1$ controller shows some oscillations as well, but the frequency is not matching that of the disturbance; the controller efficiently rejects the disturbance. This is due to the controller attempting to adapt to an ever changing condition. The peak error exhibited by the $L_1$ controlled system is significantly smaller than those achieved by the PID and MRAC controlled systems.

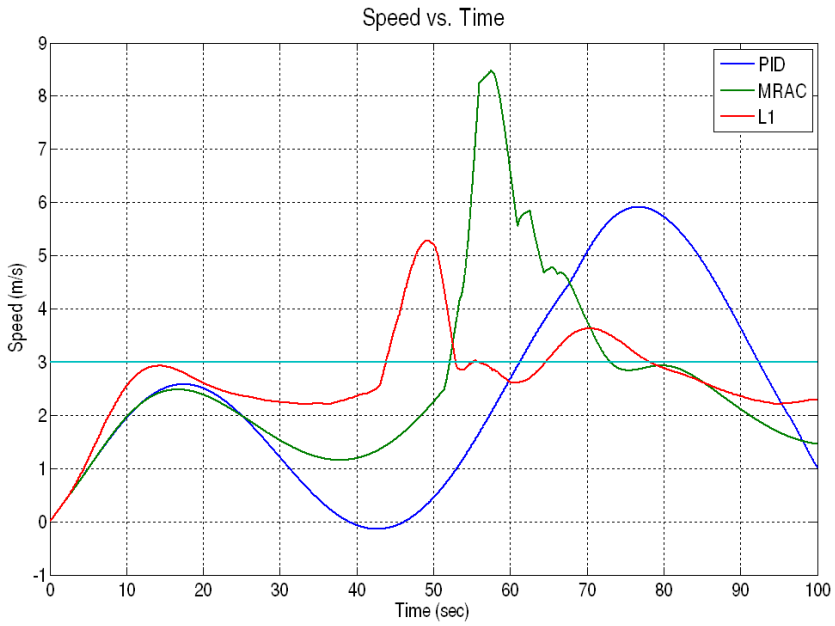


Figure 27. System Response: 3 m/s Reference Command, Oscillatory Disturbance

Figure 28 shows the control signals of the developed algorithms in the scenario above. The aggressive control signals illustrate the nature of the adaptive controllers in the presence of variable disturbances. The command signals of the MRAC and $L_1$ controllers are similar, with slightly less overall oscillations in the $L_1$ command. This result is significant because the performance of the $L_1$ based system was better than that of the MRAC based system while the control effort that was required was less.

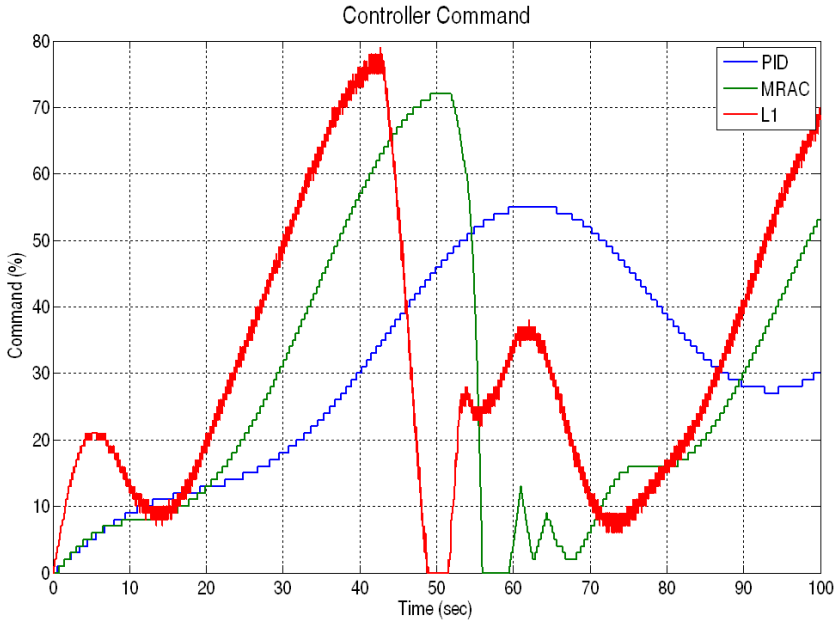


Figure 28. Controller Response: 3 m/s Reference Command, Oscillatory Disturbance

### 2. Planing Regime Results

Figure 29 shows the system responses when given reference commands of 12 m/s without a disturbance present. Both the PID and the $L_1$ controlled systems exhibit overshoots while the MRAC controlled system does not. The $L_1$ controlled system has the shortest rise time and rapidly settles with very small amplitude and low frequency oscillations about the reference command. The MRAC controlled system has a slightly longer rise time than the $L_1$ controlled system and has a similar settling and oscillation pattern. The PID controlled system performed the worst, having the longest settling time and higher amplitude oscillations.

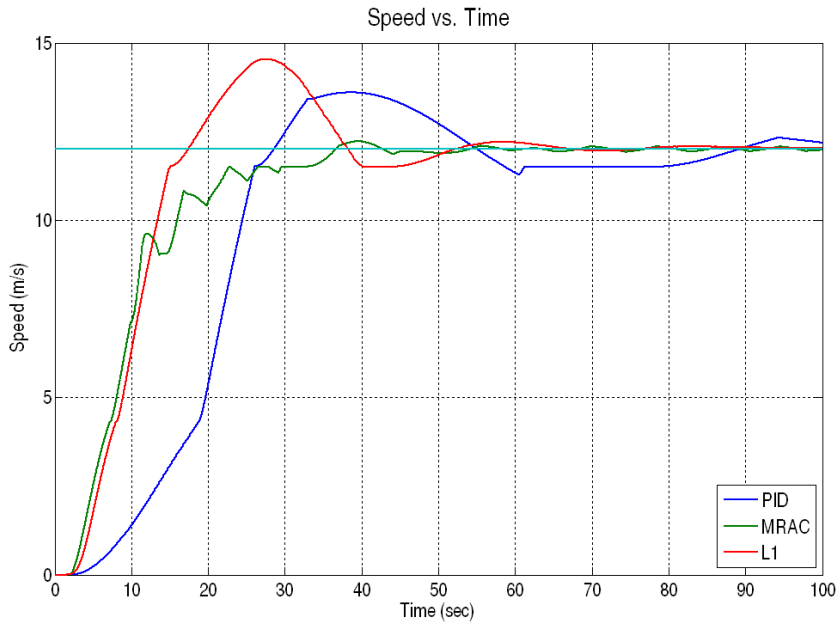


Figure 29. System Response: 12 m/s Reference Command, No Disturbance

Figure 30 shows the command signals of the controllers in the scenario above. This figure once again shows that the $L_1$ controller can achieve similar, if not better, results as the MRAC with a less taxing control effort. Again, there are small amplitude oscillations throughout the $L_1$ control signal but the adaptation loop operates much quicker than the throttle control loop. Therefore, the control signal received by the throttle controller will be much smoother and only take the overall shape of command signal.

Figure 31 shows the system responses when given reference commands of 12 m/s without a constant disturbance present as with the displacement regime simulation. The results show that the adaptive controllers, particularly the $L_1$, are capable of providing a much better response than its linear counterpart. It is worth noting that the injection of the headwind disturbance prevented the overshoot of the $L_1$ and PID controlled systems. This occurred because the disturbance brought the simulation close to the operational limits of the plant model, requiring nearly maximum control effort to reach the desired speed.

Figure 32 is the command signal for the simulation above. This plot confirms that a near maximum control effort was required to reach the desired speed. This figure also shows that the $L_1$ controlled system allows a more steady control effort.

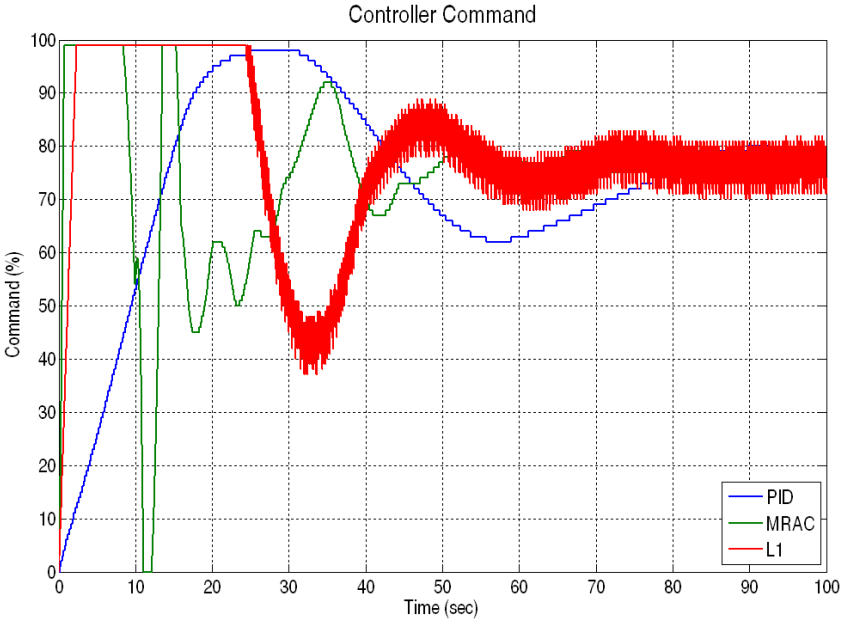


Figure 30. Controller Response: 12 m/s Reference Command, No Disturbance

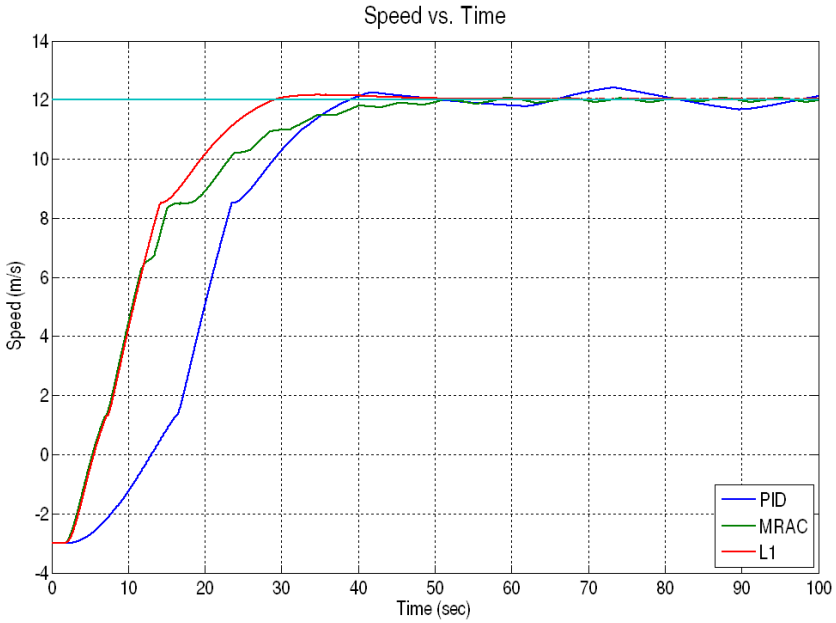


Figure 31. System Response: 12 m/s Reference Command, Constant Disturbance

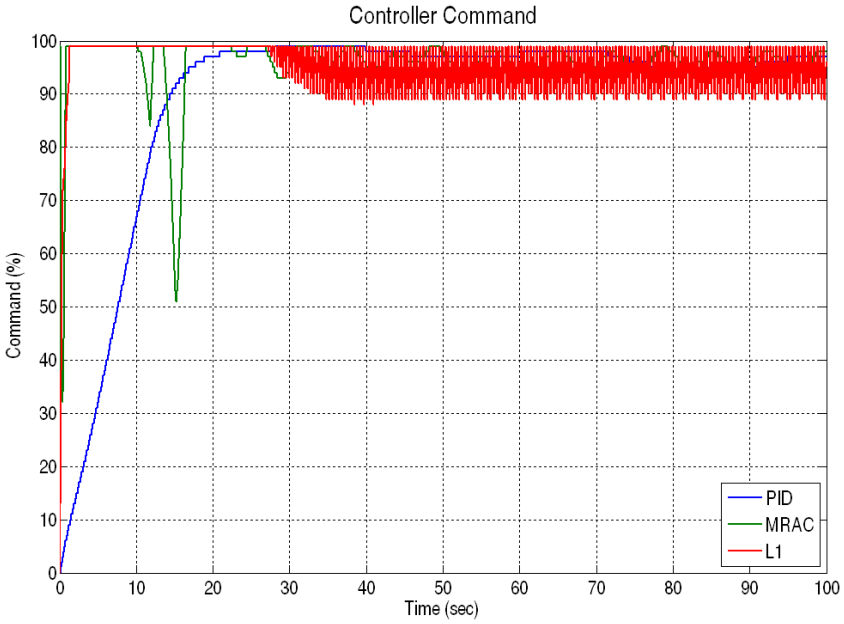


Figure 32. Controller Response: 12 m/s Reference Command, Constant Disturbance

Figures 33 and 34 show system responses and command signals for a simulation with a 12 m/s reference command and the same oscillatory disturbance as in earlier simulations. These figures show that the adaptive controllers performed better than the linear controller. As before, the $L_1$ controller performs as well as the MRAC but with a less erratic control signal.

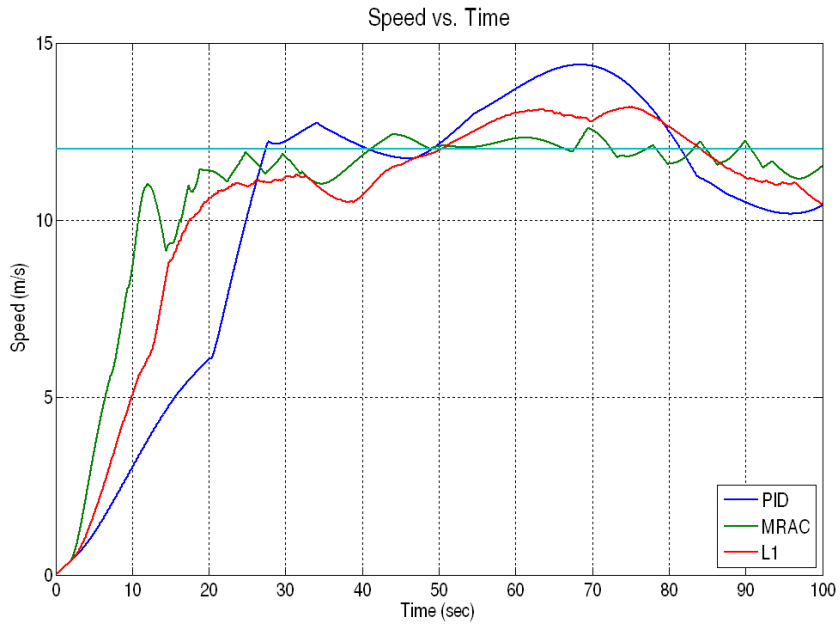


Figure 33. System Response: 12 m/s Reference Command, Oscillatory Disturbance

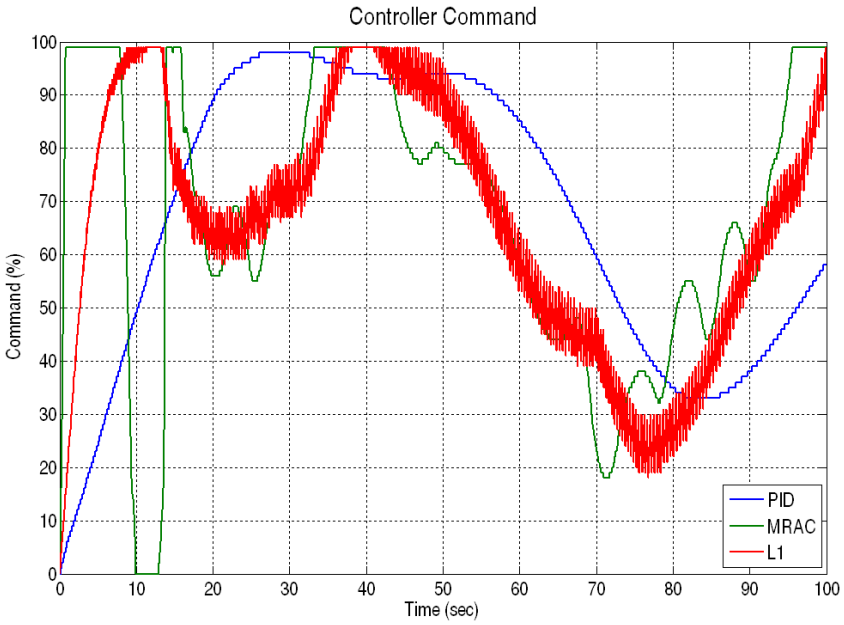


Figure 34. Controller Response: 12 m/s Reference Command, Oscillatory Disturbance

### 3. Transition Regime Results

Operating within the transition regime has been one of the goals of the controller design process. This regime has received the most interest because it is difficult for the operator to manually control the throttle to maintain a speed that lies within this regime. Figures 35 through 40 show the system performance and controller commands when the reference command is within the transition regime and the system is exposed to identical disturbances described in the previous simulations.

While previous simulations illustrated the benefit of using an adaptive controller over a standard, linear controller, there was no overwhelming advantage in implementing the $L_1$ controller over the MRAC. In the simulations in which the reference command was within the transition regime, however, the advantages of L1 become obvious.

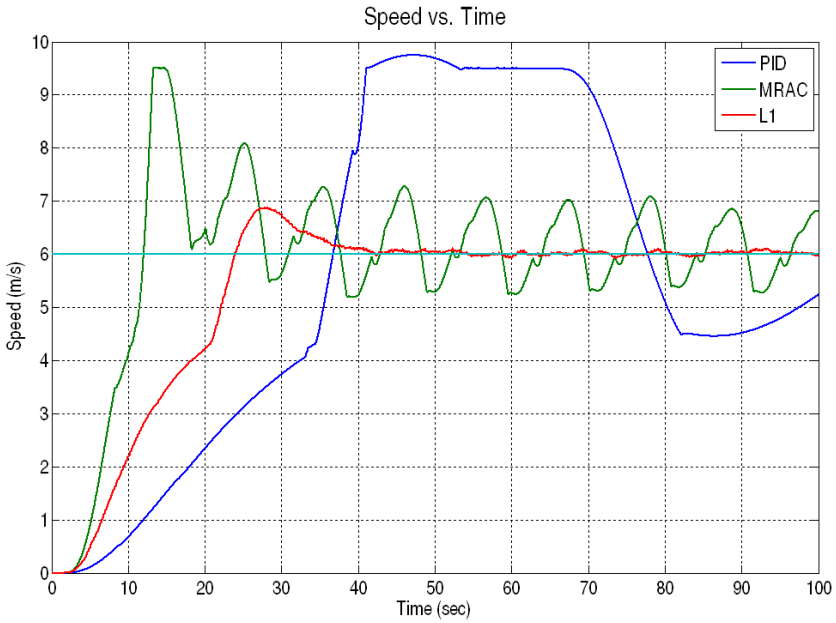


Figure 35. System Response: 6 m/s Reference Command, No Disturbance

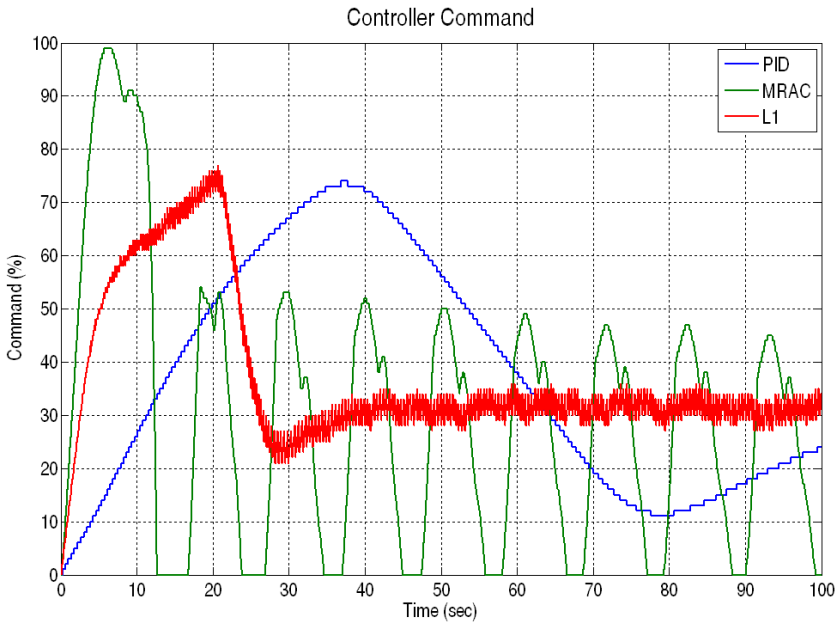


Figure 36. Controller Response: 6 m/s Reference Command, No Disturbance

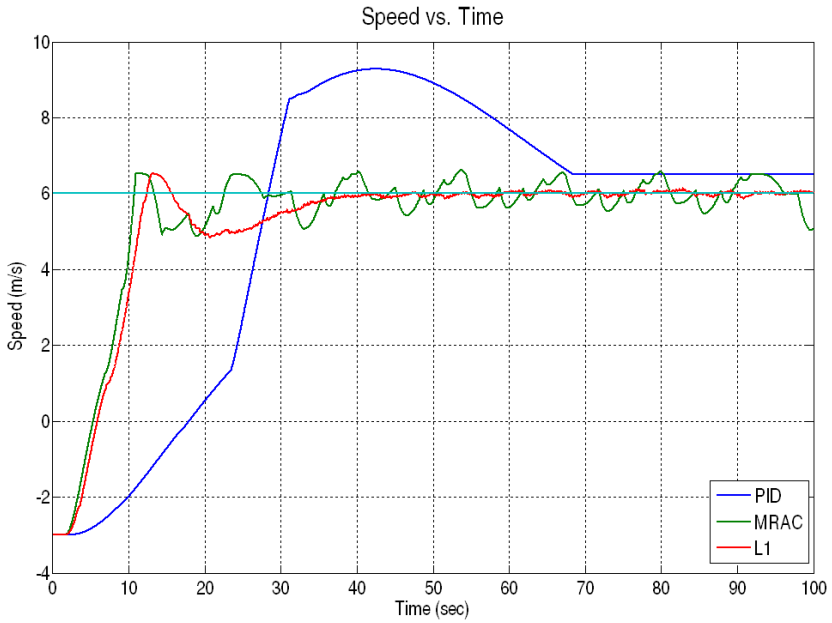


Figure 37. System Response: 6 m/s Reference Command, Constant Disturbance

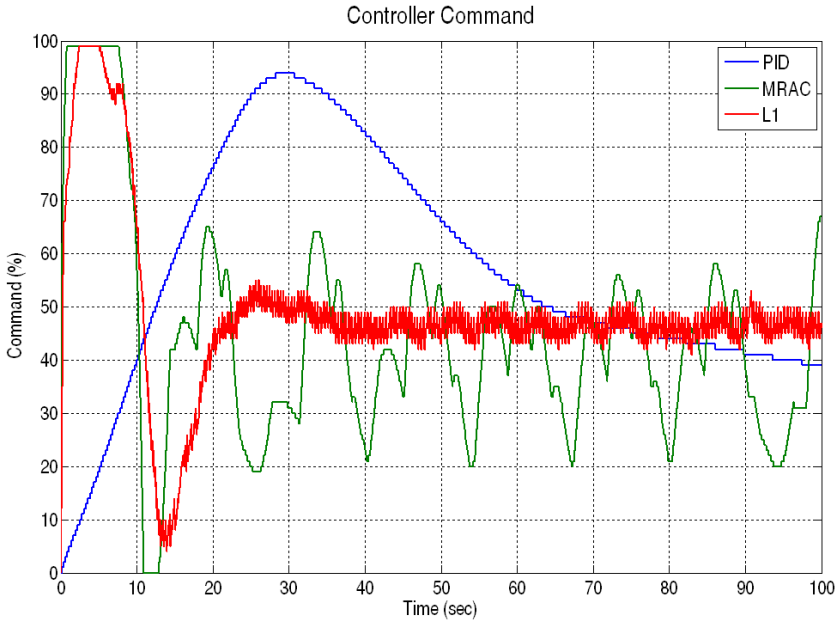


Figure 38. Controller Response: 6 m/s Reference Command, Constant Disturbance

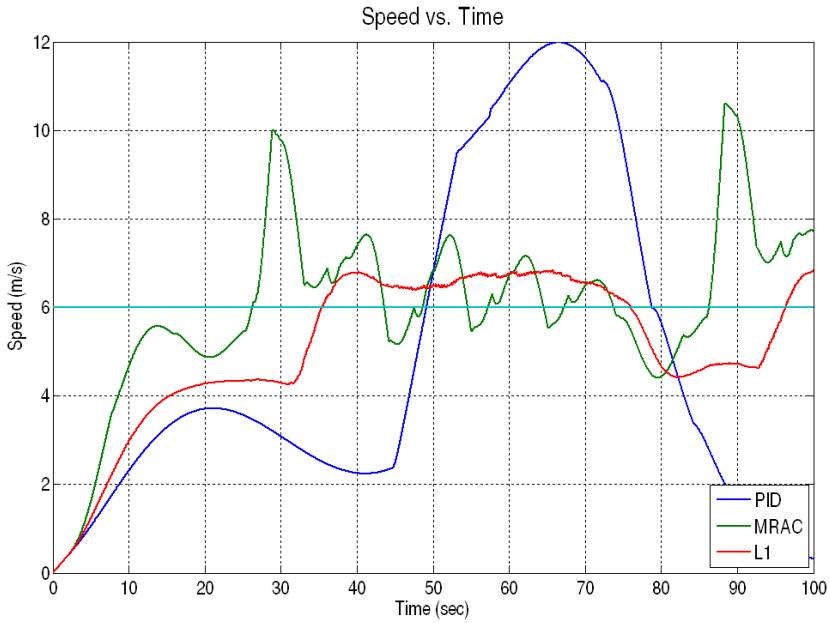


Figure 39. System Response: 6 m/s Reference Command, Oscillatory Disturbance

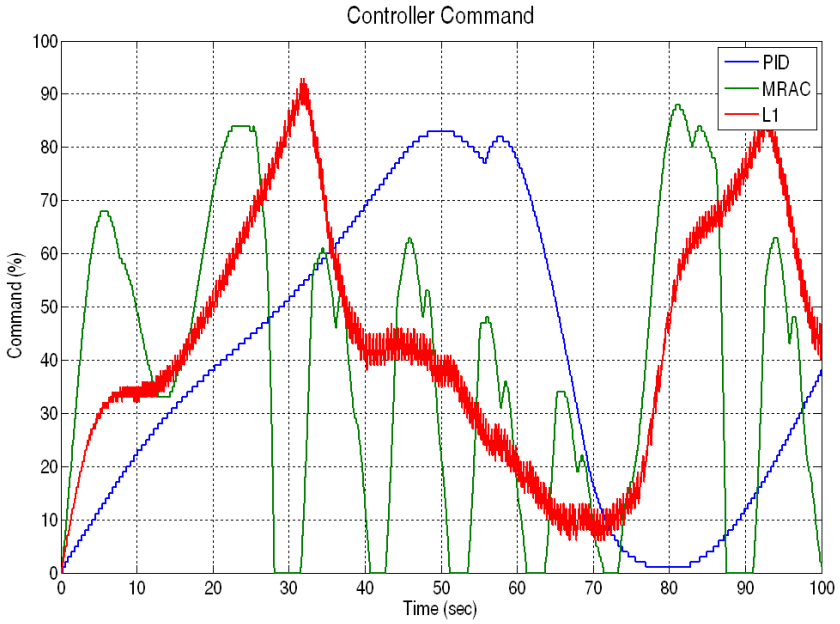


Figure 40. Controller Response: 6 m/s Reference Command, Constant Disturbance

It can be seen that the PID controller cannot maintain ASV speed anywhere near the reference command. It exhibits large oscillations about the reference command and has a very sluggish control effort. The MRAC controlled system also displays oscillations between the planing and displacement regimes, but the amplitude of these oscillations is much smaller. This improvement in performance came at the cost of a very aggressive control effort. The control effort of the MRAC has a very high frequency combined with a relatively large variation between control commands. This rapid, extreme cycling of the equipment can possibly lead to equipment failure in the future.

The $L_1$ controlled system, on the other hand, had impressive results. When operating in an environment with no disturbances or a constant disturbance, the $L_1$ controlled system was able to maintain speeds extremely close to the reference command with minimal extreme oscillations in the control signal. When exposed to an oscillatory disturbance, the $L_1$ controlled system had oscillations about the reference command but the error between the ASV speed and the reference command was relatively small and more controlled than the MRAC and PID controlled systems. The oscillations in the $L_1$

controller commands were much lower in frequency than those of the MRAC controlled system and would thereby be less detrimental to the equipment.

## C. SEA TRIAL RESULTS

Sea trials of the MRAC and PID controller were conducted on Monterey Bay. The weather conditions varied throughout the trial with scattered rain showers and ocean swells ranging from two to ten feet. The disturbances exhibited on SeaFox varied in direction and had magnitudes ranging from 0.5 to 2 m/s. These conditions made it extremely difficult when attempting to tune the controllers at sea therefore the results discussed below represent the performance of the controllers with little or no parameter differences than that in the simulation environment. In both cases, the reference commands of 3 m/s, 6 m/s and 12 m/s were used to allow for comparison between the simulation and sea trial results.

Sea trials were only conducted using the PID control and MRAC. At the time of the trials the $L_1$ controller had not been transitioned from Simulink to the ASV.

### 1. PID Results

Figures 41 and 42 show the system response and controller command with the PID controller implemented onboard SeaFox. The highlighted region represents the transition regime bounded above and below by the planing regime and the displacement regime respectively. The PID controller performed very well at maintaining a speed at 3 m/s. There was less than 1 m/s error between actual speed and the reference speed at steady state, very little variation in controller commands.

With a reference command of 12 m/s, there were large oscillations is the vessel speed with a maximum error of approximately 4 m/s. These oscillations were accompanied by larger oscillations in the controller command as compared to sea trial results at 3 m/s. The oscillations in speed response and controller command were due largely to the roughness of the seas since any disturbance in the ocean surface is amplified through the vehicle dynamics when operating in planing mode.

When issued a reference command of 6 m/s, a speed within the transition regime, the PID controller was unable to accurately maintain vessel speed. There were very large oscillations with peak error values at approximately 7.5 m/s. As expected, the control commands also had very high frequency oscillations as the controller attempted to maintain the reference speed. As with the planing speeds, rough seas played a major factor in the controller performance.


Figure 41. System Response: PID Controller Sea Trials

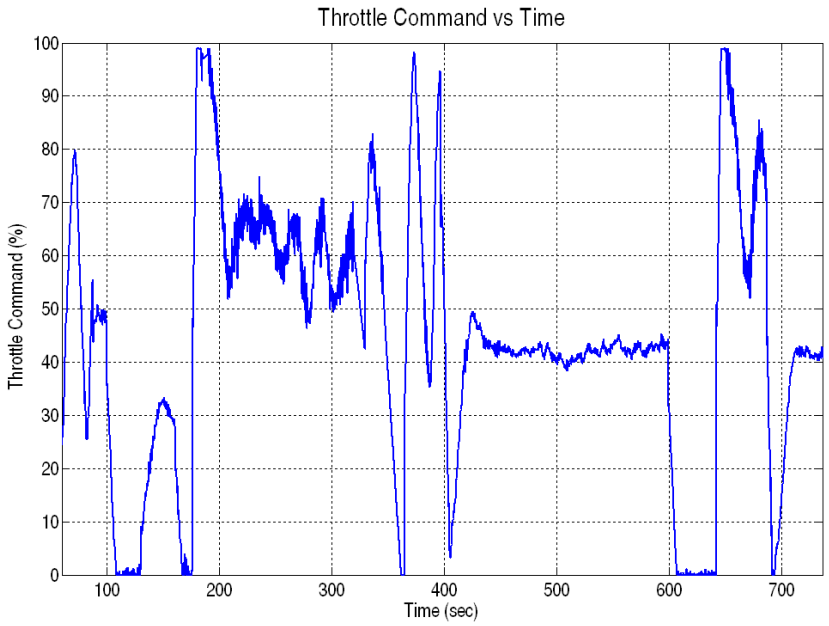


Figure 42. Controller Command: PID Controller Sea Trials

### 2. MRAC Results

Figures 43 and 44 show the system response and controller command with the MRAC controller implemented onboard SeaFox. Surprisingly the sea trial results using the MRAC did not differ much from the PID results. The MRAC also performed very well with a reference speed of 3 m/s. Again, there was less than 1 m/s error between actual speed and the reference speed at steady state, with very little variation in controller commands.

With a reference command of 12 m/s, there were still large oscillations in the vessel speed with a maximum error of approximately 4.5 m/s. The control command signal had a significantly higher frequency than that of the PID controller with the same reference command. The seas remained a problem during this set of sea trials and the aggressiveness of the MRAC appeared to have compounded the issue.

When issued a reference command of 6 m/s, the MRAC was also unable to accurately maintain the vessel speed. The speed oscillated about the reference command at a slightly higher frequency and with peak error values at approximately 9 m/s. Control commands had even higher frequency oscillations than in the case of the PID controller.

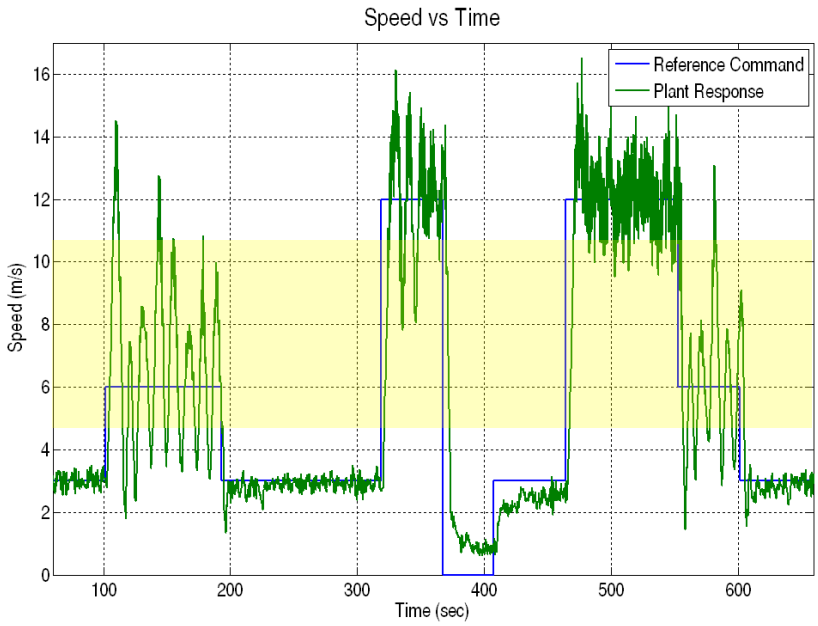


Figure 43. System Response: MRAC Sea Trials

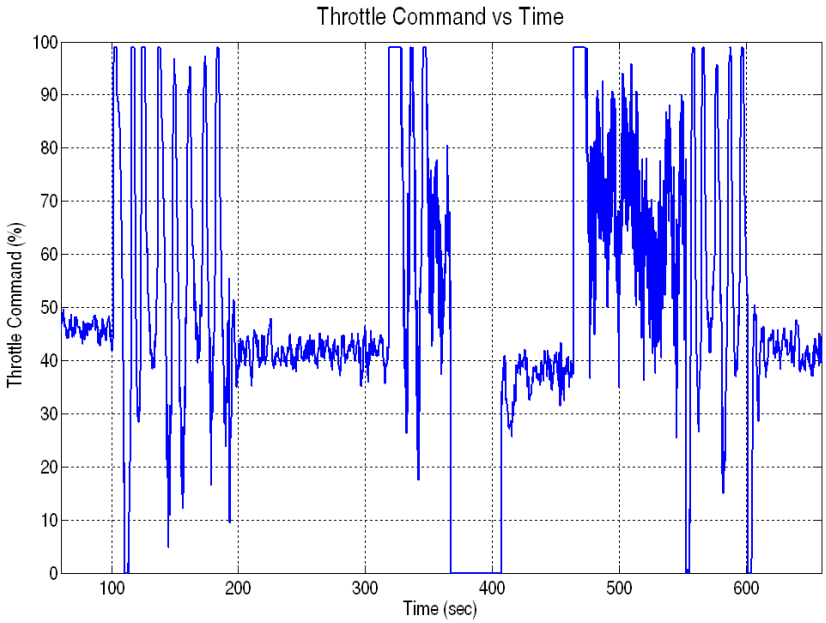


Figure 44. Controller Command: MRAC Sea Trials

THIS PAGE INTENTIONALLY LEFT BLANK

# V. CONCLUSIONS

## A. CHAPTER OVERVIEW

This chapter concludes the project with a set of summaries including an analysis of the SeaFox system identification and model construction process, control system design, and the simulation and sea trial results. This chapter also discusses possible avenues of future study.

## B. ANALYSIS

### 1. System Identification and Modeling

As expected, a significant amount of time and effort went into the development of the SeaFox mathematical model. By using two independent methods for determining the plant parameters in the different regimes, a functional mathematical representation of SeaFox operational characteristics was developed. As it was later illustrated by the experimental results, the controllers developed were functional and effective in realistic operational conditions. Thus, the underlying model has been validated to be a close representation of the actual plant characteristics. This, in turn, allows for future control development based on this mathematical model.

### 2. Simulation Results

Development of the PID, MRAC, and $L_1$ controllers was done in a Simulink design environment. The overall result of the controller development and simulation process was that the $L_1$ controller was the most versatile controller of the three. The L1 controller had better performance over all of the simulation scenarios with a significantly less demanding control effort.

The PID controller has extremely limited functionality due to its linear nature and difficulty tracking reference commands in the presence of disturbances or when the reference command is not within one of the linear regimes. Even though the control effort of the PID controller was well controlled, its relatively poor performance prohibits its use in a realistic environment.

The MRAC performed significantly better than the PID controller in simulation but in most cases this came at the cost of a very aggressive control signal. In the presence of disturbances characterized by high frequency oscillations and large changes in amplitude, the possibility of damaging mechanical equipment becomes extremely relevant.

### 3. Sea Trial Results

Sea trials were only conducted on the PID controller and the MRAC. Implementation of the L1 controller had not been completed prior to getting underway for the trials. The sea trial results show very little difference in the performance of the PID controller and MRAC. As previously stated, very little tuning was able to be accomplished during the trial due to environmental conditions.

Both controllers performed well when operating in the displacement regime but suffered in the transition and planing regimes. This was because the ASV was unable to maintain a steady interaction with the ocean surface therefore making it difficult for the controllers to successfully track the reference commands. It is believed that under better circumstances and the opportunity to properly tune the controllers, better performance can be achieved.

## C. CONCLUSION

This thesis achieved a number of objectives. First, it developed a mathematical model of the SeaFox vessel suitable for the control system design. Second, the comparative analysis of one classical LTI and two nonlinear adaptive controllers was performed to better illustrate the limitations of the control architectures and to suggest the one that is the most suitable for realistic operational conditions. It is concluded that the performance of adaptive controllers is significantly greater when compared to the linear controller. The ability to implement adaptive controllers in conjunction with the existing waypoint guidance system greatly enhances SeaFox's ability to follow projected paths at the desired speed regardless of the environmental disturbances.

## D. FUTURE WORK

In the future, it will be beneficial to tune all of the controllers in a benign environment. This will allow designers to have a better understanding of controller nominal response due to the control parameter changes and not due to environmental disturbances. This would provide the best baseline set of controller parameters for future comparison.

Once proper tuning of the controllers is complete, it would be beneficial to validate the controllers' ability to maintain reference speeds while conducting turning maneuvers. In theory, the adaptive controllers should see the change in the vehicle dynamics as a disturbance and adjust accordingly. The ability to follow nonlinear trajectories with aggressive speed profiles is essential for riverine operations.

In future work, it would also be beneficial to understand the impact of adaptive controller commands onto longevity of the system components and first of all the propulsion system. There is always a tradeoff between improved operational performance and the impact that a new control strategy has on various system components.

Finally, validation of the theory that the adaptive controllers can adjust for various mission load outs should be conducted. This is important because of the wide range of possible future applications of SeaFox. Completion of this future work will make SeaFox a more versatile autonomous asset to the Navy, capable of autonomous maneuvering in a realistic operational environment.

THIS PAGE INTENTIONALLY LEFT BLANK

# APPENDIX A.

## A. SYSTEM IDENTIFICATION TOOLBOX RESULTS

| Initial Throttle | Final Throttle | K | $\omega_n$ | ζ | % Fit |
|---|---|---|---|---|---|
| 0 | 25 | 0.064523 | 0.662603 | 1.9781 | 94.85 |
| 0 | 30 | 0.071154 | 0.651042 | 1.3108 | 90.76 |
| 0 | 40 | 0.065331 | 0.581734 | 0.91836 | 97.91 |
| 0 | 50 | 0.062034 | 1.073295 | 1.0511 | 93.94 |
| 0 | 50 | 0.062804 | 1.050277 | 0.96667 | 98.14 |
| 10 | 40 | 0.066267 | 0.983768 | 1.3294 | 95.2 |
| 20 | 40 | 0.070007 | 1.215451 | 1.5251 | 96.6 |
| 25 | 50 | 0.063904 | 1.492359 | 1.276 | 90.56 |
| 30 | 40 | 0.068798 | 0.669478 | 1.3065 | 90.85 |
| 40 | 50 | 0.064376 | 0.826993 | 1.6583 | 90.67 |
| Average: | | 0.0720571 | 0.893308 | 1.378866 | |

Table 1. Results of the System Identification for Acceleration in the Displacement Regime

| Initial Throttle | Final Throttle | K | $\omega_n$ | ζ | % Fit |
|---|---|---|---|---|---|
| 75 | 99 | 0.14212 | 0.214767 | 0.57839 | 97.89 |
| 80 | 90 | 0.15716 | 0.090152 | 0.76858 | 97.23 |
| Average: | | 0.14964 | 0.15246 | 0.673485 | |

Table 2. Results of the System Identification for Acceleration in the Planing Regime

| Initial Throttle | Final Throttle | K | $\omega_n$ | ζ | % Fit |
|---|---|---|---|---|---|
| 30 | 20 | 0.066815 | 0.045089 | 3 | 85.6 |
| 40 | 30 | 0.079491 | 1.031002 | 2.1271 | 58.31 |
| 50 | 25 | 0.048953 | 0.047339 | 3 | 77.55 |
| 50 | 40 | 0.06901 | 0.601685 | 2.8717 | 48.73 |
| 50 | 40 | 0.067376 | 0.84317 | 1.2081 | 60.28 |
| 55 | 30 | 0.080818 | 0.849185 | 2.5824 | 68.85 |
| 60 | 30 | 0.076025 | 0.235627 | 0.42368 | 42.48 |
| Average: | | 0.069784 | 0.521871 | 2.173283 | |

Table 3. Results of the System Identification for Deceleration in the Displacement Regime

| Initial Throttle | Final Throttle | K | $\omega_n$ | ζ | % Fit |
|---|---|---|---|---|---|
| 65 | 60 | 0.14309 | 0.217207 | 2.3809 | 98.65 |
| 70 | 60 | 0.49366 | 0.005413 | 3 | 85.11 |
| 99 | 75 | 0.15252 | 0.273448 | 1.1316 | 98.45 |
| Average: | | 0.26309 | 0.165356 | 2.170833 | |

Table 4. Results of the System Identification for Deceleration in the Planing Regime

## B. *FMINSEARCH* PARAMETER RESULTS

| Initial Throttle | Final Throttle | K | $\omega_n$ | ζ |
|---|---|---|---|---|
| 0 | 25 | 0.064349 | 0.30746 | 1.1116 |
| 0 | 30 | 0.070446 | 0.34291 | 0.87998 |
| 0 | 40 | 0.064948 | 0.31865 | 0.73792 |
| 0 | 50 | 0.061896 | 0.43526 | 0.77691 |
| 0 | 50 | 0.060893 | 0.43797 | 0.66332 |
| 10 | 40 | 0.066097 | 0.41283 | 0.82922 |
| 20 | 40 | 0.069881 | 0.48293 | 0.89175 |
| 25 | 50 | 0.063266 | 0.5232 | 0.77615 |
| 30 | 40 | 0.068397 | 0.84575 | 1.6396 |
| 40 | 50 | 0.06437 | 0.47089 | 1.1316 |
| Average: | | 0.065454 | 0.457785 | 0.943805 |

Table 5. *fminsearch* Parameter Results for Acceleration in the Displacement Regime

| Initial Throttle | Final Throttle | K | $\omega_n$ | ζ |
|---|---|---|---|---|
| 75 | 99 | 0.14407 | 0.25979 | 0.89739 |
| 80 | 90 | 0.15999 | 0.34856 | 1.2724 |
| Average: | | 0.15203 | 0.304175 | 1.084895 |

Table 6. *fminsearch* Parameter Results for Acceleration in the Planing Regime

| Initial Throttle | Final Throttle | K | $\omega_n$ | ζ |
|---|---|---|---|---|
| 30 | 20 | 0.0784 | 0.3795 | 1.181 |
| 40 | 30 | 0.0794 | 0.2236 | 0.8998 |
| 50 | 25 | 0.088822 | 0.50283 | 1.1633 |
| 50 | 40 | 0.069206 | 0.34116 | 1.0039 |
| 50 | 40 | 0.067427 | 0.37681 | 0.87435 |
| 55 | 30 | 0.080929 | 0.6396 | 1.8154 |
| 60 | 30 | 0.078098 | 0.34823 | 1.123 |
| Average: | | 0.077469 | 0.401676 | 1.151536 |

Table 7. *fminsearch* Parameter Results for Deceleration in the Displacement Regime

| Initial Throttle | Final Throttle | K | $\omega_n$ | ζ |
|---|---|---|---|---|
| 65 | 60 | 0.14283 | 0.1908 | 2.16 |
| 70 | 60 | 0.14439 | 0.68793 | 6.3085 |
| 99 | 75 | 0.15095 | 0.2258 | 1.0899 |
| Average: | | 0.146057 | 0.368177 | 3.186133 |

Table 8. *fminsearch* Parameter Results for Deceleration in the Planing Regime

THIS PAGE INTENTIONALLY LEFT BLANK

# APPENDIX B

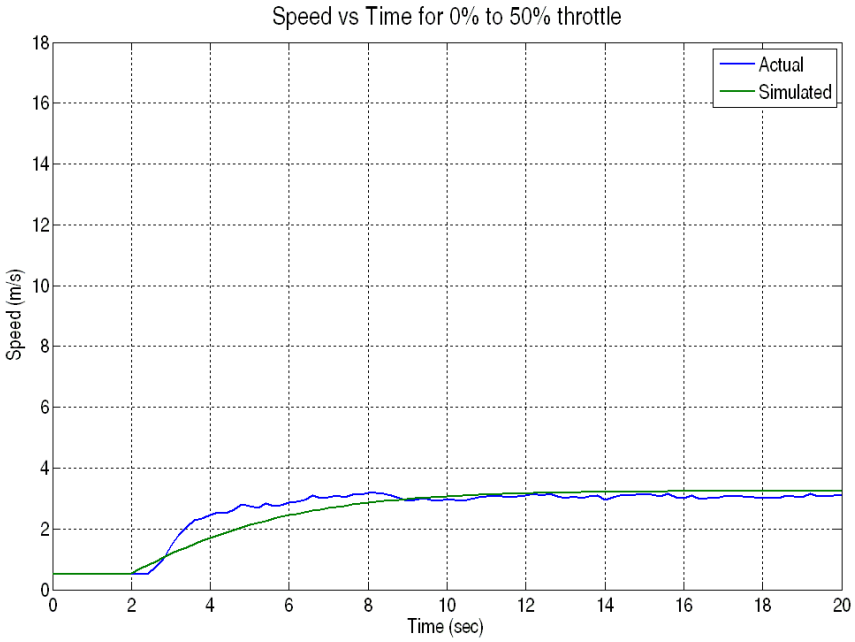


Figure 45. Model Comparison with Actual Data for a 0% to 50% Throttle Change

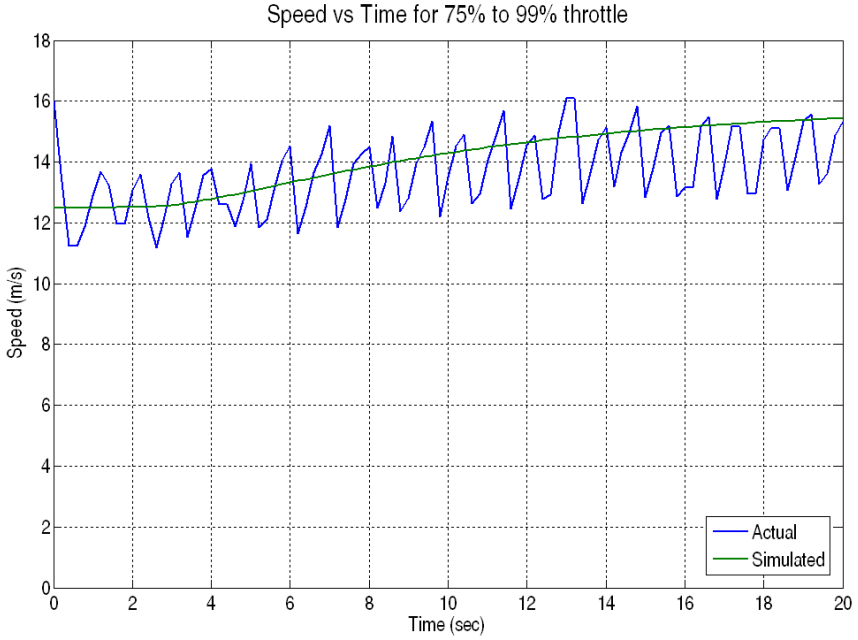


Figure 46. Model Comparison with Actual Data for a 75% to 99% Throttle Change

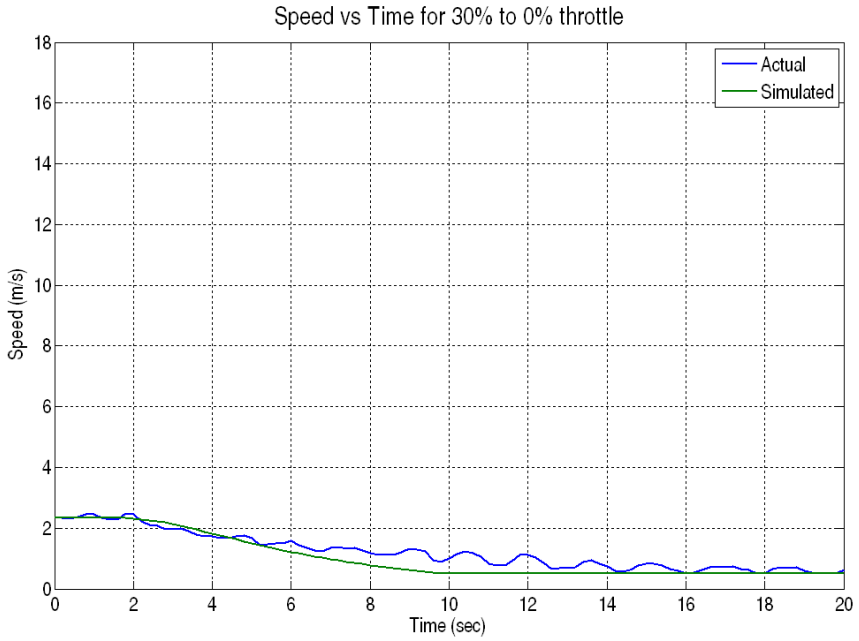


Figure 47. Model Comparison with Actual Data for a 30% to 0% Throttle Change

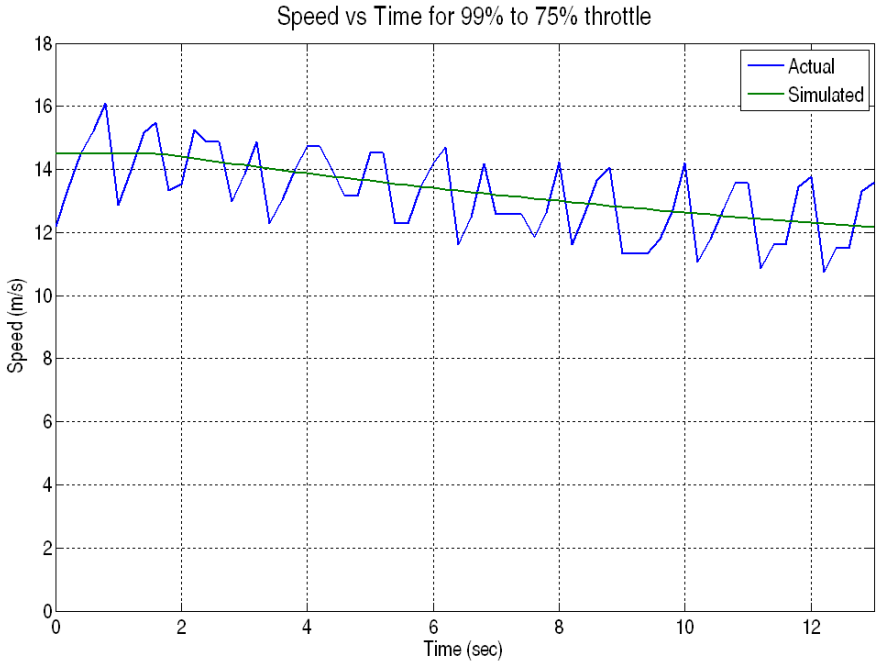


Figure 48. Model Comparison with Actual Data for a 99% to 75% Throttle Change

# APPENDIX C.

## A. EMBEDDED MATLAB FUNCTION: MAIN.M

```
x0=[1;1;1];

options=optimset('TolFun', 1e-2, 'TolX', 1e-4, 'Display', 'iter');

[x,fval]=fminsearch(@Simulation,x0)
```

## B. EMBEDDED MATLAB FUNCTION: SIMULATION.M

```
function f = Simulation(x0)

Variable1=x0(1);
Variable2=x0(2);
Variable3=x0(3);

opt = simset('SrcWorkspace', 'Current');
sim('Model_Name', [0 run_time], opt);
f=sum(simout1(:,1).^2);
```

THIS PAGE INTENTIONALLY LEFT BLANK

# APPENDIX D.

## A. PID CONTROLLER PARAMETERS

| Region | $K_p$ | $K_i$ | $K_d$ | N |
|---|---|---|---|---|
| Low Speed (<10 m/s) | 1.0003 | 1.011 | 1.0425 | 1.000 |
| High Speed (≥10 m/s) | 1.3451 | 0.98348 | 1.0177 | 1.000 |

Table 9. Parameters of the PID Controller

## B. COMPOSITE MRAC CONTROLLER PARAMETERS

| Region | $\gamma$ | $\gamma_x$ | $\gamma_r$ | $\gamma_u$ | $a_p$ |
|---|---|---|---|---|---|
| Low Speed (<10 m/s) | 10 | 0.01 | 0.05 | 0.5 | -0.6 |
| High Speed (≥10 m/s) | 10 | 0.01 | 0.05 | 0.5 | -1.6 |

Table 10. Parameters of the Composite MRAC Controller

## C. $L_1$ CONTROLLER PARAMETERS

| | |
|---|---|
| $\Gamma$ | 10000 |
| k | 600 |
| D(s) | $\frac{1}{s^2+40s+0.001}$ |
| $\hat{\omega}$ bound radius | 0.225 |
| $\hat{\omega}$ center of bound | 0.2125 |
| $\hat{\theta}$ bound radius | 0.225 |
| $\hat{\theta}$ center of bound | 0 |
| $\hat{\sigma}$ bound radius | 0.225 |
| $\hat{\sigma}$ center of bound | 0 |

Table 11. Parameters of the $L_1$ Controller

THIS PAGE INTENTIONALLY LEFT BLANK

# LIST OF REFERENCES


[1] "The Navy Unmanned Surface Vehicle (USV) Master Plan." Internet: http://www.navy.mil/navydata/technology/usvmppr.pdf, Jul. 23, 2007 [Mar 15, 2012].

[2] "FY 2009-2034 Unmanned Systems Integrated Roadmap," Internet: http://www.acq.osd.mil/psa/docs/UMSIntegratedRoadmap2009.pdf, [Mar 15, 2012].

[3] A. Gadre, S. Kragelund, T. Masek, D. Stilwell, C. Woolsey, and D. Horner, "Subsurface and surface sensing for autonomous navigation in a riverine environment," in *Proceedings of the Association of Unmanned Vehicle Systems International (AUVSI) Unmanned Systems North America 2009*, 2009, vol. 2, p. 1192.

[4] R. Marshall, *All About Power Boats*. Blacklick, OH: McGraw-Hill Companies, 2002, pp. 4–5.

[5] M. S. Triantafyllou and F. S. Hover, "Maneuvering and control of marine vehicles," Massachussets Institute of Technology, Tech. Rep., 2002.

[6] T. I. Fossen, *Marine Control Systems*. Trodheim, Norway: Marine Cybernetics, 2002, p. 570.

[7] D. Savitsky, "Planing Craft," *Naval Engineers Journal*, vol. 97, pp. 113–141, 1985.

[8] K. Ogata, *Modern Control Engineering*, 4th ed. Upper Saddle River, NJ: Prentice Hall, 2002.

[9] L. Ljung, *System Identification: Theory for the User*, 2nd ed. Upper Saddle River, NJ: Prentice Hall, 1999.

[10] J. Yang, W. Y., Cao, W., Chung, T.-S. and Morris, J., *Applied Numerical Methods using MATLAB*. Hoboken, NJ: John Wiley & Sons, Inc., 2005.

[11] B. Hunt, *A Guide to MATLAB: For Beginners and Experienced Users*, 2nd ed. Cambridge, Massachusetts USA: Cambridge University Press, 2006.

[12] J. Lagarias, J. Reeds, M. Wright, and P. Wright, "Convergence properties of the Nelder-Mead simplex method in low dimensions," *SIAM Journal of Optimization*, vol. 9, no. 1, pp. 112–147, 1998.

[13] K. J. Åström and T. Hägglund, *PID controllers*, vol. 2. Research Triangle Park, N.C.: International Society for Measurement and Control, 1995, p. 343.

[14] K. J. Åström and B. Wittenmark, *Adaptive control*, vol. 2. Reading, MA.: Addison-Wesley, 1995, p. 574.

[15] B. Ioannou, and P. Fidan, *Adaptive Control Tutorial*. Cambridge, MA: Cambridge University Press, 2006.

[16] M. Duarte and K. Narendra, "Combined direct and indirect approach to adaptive control," *IEEE Transactions on Automatic Control*, vol. 34, no. 10, pp. 1071–1075, 1989.

[17] S. Karason and A. Annaswamy, "Adaptive control in the presence of input constraints," *IEEE Transactions on Automatic Control*, vol. 39, no. 11, pp. 2325–2330, 1994.

[18] N. Hovakimyan, and C. Cao, *L1 Adaptive Control Theory: Guaranteed Robustness with Fast Adaptation*. Philadelphia, PA: Society for Industrial and Applied Mathematics, 2010a.

[19] N. Hovakimyan and C. Cao, "Stability margins of L1 adaptive control architecture," *IEEE Transactions on Automatic Control*, vol. 55, no. 2, pp. 480–487, 2010b.

[20] N. Hovakimyan and C. Cao, "Adaptive controller for systems with unknown time-varying parameters and disturbances in the presence of non-zero trajectory initialization error," *International Journal of Control*, vol. 81, no. 7, pp. 1147–1161, 2008.

# INITIAL DISTRIBUTION LIST

1. Defense Technical Information Center
   Ft. Belvoir, Virginia

2. Dudley Knox Library
   Naval Postgraduate School
   Monterey, California

3. Professor Vladimir Dobrokhodov
   Department of Mechanical and Aeronautical Engineering
   Naval Postgraduate School
   Monterey, California

4. Research Associate Professor Douglas P. Horner
   Center for Autonomous Vehicle Research (CAVR)
   Naval Postgraduate School
   Monterey, California

5. Professor Oleg Yakimenko
   Department of Mechanical and Aeronautical Engineering
   Naval Postgraduate School
   Monterey, California

6. Professor Isaac Kaminer
   Department of Mechanical and Aeronautical Engineering
   Naval Postgraduate School
   Monterey, California